Global-scale distribution of ozone in the remote troposphere from ATom and HIPPO airborne field missions.

Ilann Bourgeois[1,2], Jeff Peischl[1,2], Chelsea R. Thompson[1,2], Kenneth C. Aikin[1,2], Teresa Campos[3], Hannah Clark[4], Róisín Commane[5], Bruce Daube[6], Glenn W. Diskin[7], James W. Elkins[8], Ru-Shan Gao[2], Audrey Gaudel[1,2], Eric J. Hintsa[1,8], Bryan J. Johnson[8], Rigel Kivi[9], Kathryn McKain[1,8], Fred L. Moore[1,8], David D. Parrish[1,2], Richard Querel[10], Eric Ray[1,2], Ricardo Sánchez[11], Colm Sweeney[8], David W. Tarasick[12], Anne M. Thompson[13], Valérie Thouret[14], Jacquelyn C. Witte[3], Steve C. Wofsy[6], and Thomas B. Ryerson[2].

[1]Cooperative Institute for Research in Environmental Sciences, University of Colorado Boulder, Boulder, CO, USA
[2]NOAA CSL, Boulder, CO, USA
[3]National Center for Atmospheric Research, Boulder, CO, USA
[4]IAGOS-AISBL, Brussels, Belgium
[5]Department of Earth and Environmental Sciences, Lamont-Doherty Earth Observatory of Columbia University, New York, NY, USA
[6]School of Engineering and Applied Sciences, Harvard University, Cambridge, MA, USA
[7]NASA Langley Research Center, Hampton, VA, USA
[8]NOAA GML, Boulder, CO, USA
[9]Finnish Meteorological Institute, Space and Earth Observation Centre, Sodankylä, Finland
[10]National Institute of Water & Atmospheric Research (NIWA), Lauder, NZ
[11]Servicio Meteorológico Nacional, Buenos Aires, Argentina
[12]Experimental Studies Research Division, MSC/Environment and Climate Change Canada, Downsview, Ontario, CA
[13]Earth Sciences Division, NASA/Goddard Space Flight Center, Greenbelt, MD, USA
[14]Laboratoire d'Aérologie, CNRS and Université Paul Sabatier, Université de Toulouse, Toulouse, FR

Abstract

Ozone is a key constituent of the troposphere where it drives photochemical processes, impacts air quality, and acts as a climate forcer. Large-scale in situ observations of ozone commensurate with the grid resolution of current Earth system models are necessary to validate model outputs and satellite retrievals. In this paper, we examine measurements from the Atmospheric Tomography (ATom, 4 deployments in 2016–2018) and the HIAPER Pole-to-Pole Observations (HIPPO; 5 deployments in 2009–2011) experiments, two global-scale airborne campaigns covering the Pacific and Atlantic basins.

ATom and HIPPO represent the first global-scale, vertically resolved measurements of O_3 distributions throughout the troposphere, with HIPPO sampling the atmosphere over the Pacific and ATom sampling both the Pacific and Atlantic. Given the relatively limited temporal resolution of these two campaigns, we first compare ATom and HIPPO ozone data to longer-term observational records to establish the representativeness of our dataset. We show that these two airborne campaigns captured on average 53, 54, and 38 % of the ozone variability in the marine boundary layer, free troposphere, and upper troposphere/lower stratosphere (UTLS), respectively, at nine well-established ozonesonde sites. Additionally, ATom captured the most frequent ozone concentrations measured by regular commercial aircraft flights in the northern Atlantic UTLS. We then use the repeated vertical profiles from these two campaigns to confirm and extend the existing knowledge ~~global-scale picture~~ of tropospheric ozone spatial and vertical distributions throughout the remote troposphere. We highlight a clear hemispheric gradient, with greater ozone in the northern hemisphere, consistent with greater precursor emissions and consistent with previous modeling and satellite studies. We also show that the ozone distribution below 8 km was similar in the extra-tropics of the Atlantic and Pacific basins, likely due to zonal circulation patterns. However, twice as much ozone was found in the tropical Atlantic than in the tropical Pacific, due to well-documented dynamical patterns transporting continental air masses over the Atlantic. Finally, we show that the seasonal variability of tropospheric ozone over the Pacific and the Atlantic basins is driven year-round by transported continental plumes and photochemistry, and the vertical distribution is driven by photochemistry and mixing with stratospheric air. This new dataset provides additional constraints for global climate and chemistry models to improve our understanding of both ozone production and loss processes in remote regions, as well as the influence of anthropogenic emissions on baseline ozone.

1. Introduction

Tropospheric ozone (O_3) plays a major role in local, regional, and global air quality and significantly influences Earth's radiative budget (IPCC, 2013; Shindell et al., 2012). In addition, O_3 drives tropospheric photochemical processes by controlling hydroxyl radical (OH) abundance, which subsequently controls the lifetime of other pollutants including volatile organic compounds (VOCs), methane, and some stratospheric ozone-depleting substances (Crutzen, 1974; Levy, 1971). Sources of O_3 to the troposphere include downward transport from the stratosphere (Junge, 1962) and photochemical production from precursors such as carbon monoxide (CO), methane (CH_4), and VOCs in the presence of nitrogen oxides (NO_x) from natural or anthropogenic sources (Monks et al., 2009). Tropospheric O_3 sinks include photo-dissociation, chemical reactions, and dry deposition. Owing to its relatively long lifetime (~23 days in the troposphere; Young et al., 2013), O_3 can be transported across hemispheric scales. O_3 mixing ratios over a region thus depend not only on local and regional sources and sinks, but also on long-range transport. Further, the uneven density of O_3 monitoring locations around the globe leads to significant sampling gaps, especially near developing nations and away from land (Gaudel et al., 2018). The troposphere over the remote oceans is among the least-sampled regions, despite hosting 60–70 % of the global tropospheric O_3 burden (Holmes et al., 2013).

Since the early 1980's, several aircraft campaigns have addressed this paucity of remote observations, most notably under the umbrella of the Global Tropospheric Experiment (GTE), a major component of the National Aeronautics and Space Administration (NASA) Tropospheric Chemistry Program (https://eosweb.larc.nasa.gov/project/gte/gte_table). Airborne campaigns have targeted both the Pacific and Atlantic Oceans, providing novel characterization of O_3 sources, distribution, and photochemistry in the marine troposphere (Browell et al., 1996a; Davis et al., 1996; Jacob et al., 1996; Pan et al., 2015; Schultz et al., 1999; Singh et al., 1996c) and the low-O_3 tropical Pacific pool (Singh et al., 1996b), the pervasive role of continental outflow on O_3 production (Bey et al., 2001; Crawford et al., 1997; Heald et al., 2003; Kondo et al., 2004; Martin et al., 2002; Zhang et al., 2008), and the marked influence of African and South American biomass burning on O_3 production in the Southern Hemisphere (Browell et al., 1996b; Fenn et al., 1999; Mauzerall et al., 1998; Singh et al., 1996a; Thompson et al., 1996). Ozonesondes have been launched from remote sites for more than three decades in some places, and have provided additional constraints on the sources and photochemical balance of

tropospheric O_3, including a deep understanding of the vertically-resolved tropospheric O_3 climatology in select locations (Derwent et al., 2016; Diab et al., 2004; Jensen et al., 2012; Kley et al., 1996; Liu et al., 2013; Logan, 1985; Logan and Kirchhoff, 1986; Newton et al., 2017; Oltmans et al., 2001; Parrish et al., 2016; Sauvage et al., 2006; Thompson et al., 2012). Spatially-resolved O_3 climatology has been provided by routine sampling by commercial aircraft, but has mostly been limited to the upper troposphere or over continental regions (Clark et al., 2015; Cohen et al., 2018; Logan et al., 2012; Petetin et al., 2016; Sauvage et al., 2006; Thouret et al., 1998; Zbinden et al., 2013), and by satellite observations (Edwards et al., 2003; Fishman et al., 1990, 1991; Hu et al., 2017; Thompson et al., 2017; Wespes et al., 2017; Ziemke et al., 2005, 2006, 2017), somewhat tempered by large uncertainties (Tarasick et al., 2019b). Recent overview analyses depict the current understanding of global tropospheric O_3 sources, distribution, and photochemical balance and underscore the insufficiency of observations in the remote free troposphere (Cooper et al., 2014; Gaudel et al., 2018; Tarasick et al., 2019b) necessary to improve the current representation of tropospheric O_3 in global chemical models (Young et al., 2018). Spatial and temporal representativeness of O_3 observations is currently the biggest source of uncertainty when inferring O_3 climatology in the free troposphere, even in regions where observation are abundant but not ideally distributed (Lin et al., 2015b; Tarasick et al., 2019b). Most studies reporting global O_3 distribution use satellite observations (Edwards et al., 2003; Fishman et al., 1990, 1991; Thompson et al., 2017; Wespes et al., 2017; Ziemke et al., 2005, 2006, 2017), modeling analyses (Hu et al., 2017), or observations spatially expanded using back trajectory calculations (e.g., Liu et al., 2013; Tarasick et al., 2010). While useful, these studies come with somewhat large uncertainties, as recently noted by reports from the Tropospheric Ozone Assessment Report (TOAR), and thus require additional in situ observations to be used as a validation bench-mark (Tarasick et al., 2019b; Young et al., 2018).

The Atmospheric Tomography mission (ATom, https://espo.nasa.gov/atom) was a NASA Earth Venture airborne field project to address the sparseness of atmospheric observations over remote ocean regions by systematically sampling the troposphere over the Pacific and Atlantic basins along a global-scale circuit (Fig. 1). ATom deployed an extensive payload on the NASA DC-8 aircraft, measuring a wide range of chemical, microphysical, and meteorological parameters in repeated vertical profiles from 0.2 km to over 13 km altitude, from the Arctic to the Antarctic over the Pacific and Atlantic Oceans, in four separate seasons from 2016 to 2018.

ATom built on a previous study, the HIAPER Pole-to-Pole Observations mission (HIPPO, https://www.eol.ucar.edu/field_projects/hippo). The goal of HIPPO was to measure atmospheric distributions of important greenhouse gases and reactive species over the Pacific Ocean, from the surface to the tropopause, five times during different seasons from 2009 to 2011. Together, ATom and HIPPO provide recent and comprehensive information about the altitudinal, latitudinal, and seasonal composition of the remote troposphere over the Pacific, and over the Atlantic for ATom. In addition, ATom and HIPPO sampling strategies were designed to deliver an objective climatology of key species to enable modelling of air parcel reactivity of the remote troposphere (Prather et al., 2017).

Here we use existing ozonesonde and commercial aircraft observations of O_3 at selected locations along the ATom and HIPPO circuits to provide a climatological context for the altitudinal, latitudinal, and seasonal distributions of O_3 derived from the systematic airborne in situ "snapshots". Long-term O_3 observations are obtained from decades of ozonesonde vertical profiles (e.g., Oltmans et al., 2013; Thompson et al., 2017) and from ~60,000 flights using the In-service Aircraft for a Global Observing System (IAGOS) infrastructure (Petzold et al., 2015; http://www.iagos.org). Ozonesondes have typically been launched weekly for two decades or more, depending on the site, and have sampled a wide range of air masses across the globe, from O_3-poor remote surface locations to the O_3-rich stratosphere. IAGOS commercial aircraft have provided daily measurements in the upper troposphere and lower stratosphere (UTLS) for the past 25 years, especially over the northern midlatitudes between America and Europe. Combined, the ozonesonde and IAGOS datasets offer robust measurement-based climatologies that quantify the full expected range of atmospheric O_3 variability with altitude and season. The in-situ data from temporally-limited intensive field studies can be placed in context by comparing them with long-term ozonesonde and commercial aircraft monitoring data. Evaluating the representativeness of in situ observations from airborne campaigns by comparing them to longer-term observational records is a critical exercise never before done at such a global scale. We show that ATom and HIPPO measurements capture the spatial and, in some cases, temporal dependence of O_3 in the remote atmosphere, thus highlighting the usefulness of airborne observations to fill in the gaps of established but limited O_3 climatologies and other similarly long-lived species. Then, we use the geographically extensive ATom and HIPPO vertical profile

data to establish a more complete measurement-based benchmark for O_3 abundance and distribution in the remote marine atmosphere.

2. Measurements

2.1 ATom

The four ATom circuits occurred in July–August 2016 (ATom-1), January–February 2017 (ATom-2), September–October 2017 (ATom-3), and April–May 2018 (ATom-4), thus spanning all four seasons in both hemispheres over a two-year timeframe (Table S1). The mission in total consisted of 48 science flights and 548 vertical profiles distributed nearly equally along the global circuit. All four deployments completed roughly the same loop, starting and ending in Palmdale, California, USA (Fig. 1). A notable addition during ATom-3 and -4 were out-and-back flights from Punta Arenas, Chile to sample the Antarctic troposphere and UTLS.

O_3 was measured using the National Oceanic and Atmospheric Administration (NOAA) nitrogen oxides and ozone (NO_yO_3) instrument. The O_3 channel of the NO_yO_3 instrument is based on the gas-phase chemiluminescence (CL) detection of ambient O_3 with pure NO added as a reagent gas (Ridley et al., 1992; Stedman et al., 1972). Ambient air is continuously sampled from a pressure-building ducted aircraft inlet into the NO_yO_3 instrument at a typical flow rate of 1025.0 ± 0.2 standard cubic centimeters per minute (sccm) in flight. Pure NO reagent gas flow delivered at 3.450 ± 0.006 sccm is mixed with sampled air in a pressure (8.00 ± 0.08 Torr) and temperature (24.96 ± 0.01 °C) controlled reaction vessel. NO-induced CL is detected with a dry-ice-cooled, red-sensitive photomultiplier tube and the amplified digitized signal recorded using an 80 MHz counter; pulse coincidence corrections at high count rates were applied, but are negligible for the data presented in this work. The instrument sensitivity for measuring O_3 under these conditions is 3150 ± 80 counts per second per part per billion by volume (ppbv) averaged over the entire ATom circuit. CL detector calibrations were routinely performed both on the ground and during flight by standard addition of O_3 produced by irradiating ultrapure air with 185 nm UV light and independently measured using UV optical absorption at 254 nm. All O_3 measurements were taken at a temporal resolution of 10 Hz, averaged to 1 Hz, and corrected for the dependence of instrument sensitivity on ambient water vapor content (Ridley et al., 1992). Under these conditions the total estimated 1 Hz uncertainty at sea level is ± (0.015 ppbv + 2 %).

157 A commercial dual-beam photometer (2B Technologies model 211) based on UV optical
158 absorption at 254 nm also measured O_3 on ATom, with an estimated uncertainty of ± (1.5 ppbv +
159 1 %) at a 2-second sampling resolution. Comparison of the 2B absorption instrument O_3 data to
160 the NO_yO_3 CL instrument O_3 data agreed to within combined instrumental uncertainties, lending
161 additional confidence to the NO_yO_3 CL instrument calibration. For the ATom project we use
162 NO_yO_3 instrument O_3 data in the following analyses.
163 Data from two CO measurements were combined in this analysis. The Harvard quantum
164 cascade laser spectrometer (QCLS) instrument used a pulsed quantum cascade laser tuned at
165 ~2160 cm^{-1} to measure the absorption of CO through an astigmatic multi-pass sample cell with
166 76 m path length and detection using a liquid-nitrogen-cooled HgCdTe detector (Santoni et al.,
167 2014). In-flight calibrations were conducted with gases traceable to the NOAA World
168 Meteorological Organization (WMO) X2014A scale, and the QCLS observations have an
169 accuracy and precision of 3.5 and 0.15 ppb for 1 Hz data, respectively. CO was also measured by
170 the NOAA cavity ring-down spectrometer (CRDS, Picarro, Inc., model G2401-m; Karion et al.,
171 2013) in the 1.57 μm region with a total uncertainty of 5.0 ppbv for 1 Hz data. The NOAA
172 Picarro data were also reported on the Wolrd Meteorological Organization (WMO) X2014A
173 scale. The combined CO data (CO-X) used here corresponds to the QCLS data, with the Picarro
174 measurement used to fill calibration gaps in the QCLS time series.
175 Water (H_2O) vapor was measured using the NASA Langley Diode Laser Hygrometer
176 (DLH), an open-path infrared absorption spectrometer that uses a laser locked to a water vapor
177 absorption feature at ~1.395 μm. Raw data are processed at the instrument's native ~100 Hz
178 acquisition rate and averaged to 1 Hz with an overall measurement accuracy within 5 %.
179
180 2.2 HIPPO
181 The HIPPO mission consisted of five seasonal deployments over the Pacific basin
182 between 2009 and 2011, from the North Pole to the coastal waters of Antarctica (Wofsy, 2011).
183 HIPPO deployments consisted of two transects, southbound and northbound, and occurred in
184 January 2009 (HIPPO-1), October–November 2009 (HIPPO-2), March–April 2010 (HIPPO-3),
185 June–July 2011 (HIPPO-4) and August–September 2011 (HIPPO-5). The platform used was the
186 NSF Gulfstream V (GV) aircraft. More details can be found in Table S1.

187 A NOAA custom-built dual-beam photometer based on UV optical absorption at 254 nm
188 was used to measure O_3 (Proffitt and McLaughlin, 1983). The uncertainty of the 1 Hz O_3 data is
189 estimated to be ± (1 ppbv + 5 %) for 1 Hz data. A commercial dual-beam O_3 photometer (2B
190 Technologies model 205) based on UV optical absorption at 254 nm was also included in the
191 HIPPO payload. Comparison of the 2B O_3 data to the NOAA O_3 data showed general agreement
192 within combined instrument uncertainties on level flight legs. For the HIPPO project we use
193 NOAA O_3 data in the following analyses.
194 Data from two CO measurements were combined in this analysis. The QCLS instrument
195 was the same instrument as used during ATom and described in section 2.1. CO was also
196 measured by an Aero-Laser AL5002 instrument using vacuum UV resonance fluorescence (in
197 the 170–200 nm range) instrument with an uncertainty of ± (2 ppbv + 3 %) at a 2-second
198 sampling resolution. The combined CO data (CO-X) used here corresponds to the QCLS data,
199 with the Aero-Laser measurement used to fill calibration gaps in the QCLS time series.
200
201 2.3 IAGOS
202 IAGOS is a European Research Infrastructure that provides airborne in situ chemical,
203 aerosol, and meteorological measurements using commercial aircraft (Petzold et al., 2015). The
204 IAGOS Research Infrastructure includes data from both the CARIBIC (Civil Aircraft for the
205 Regular Investigation of the atmosphere Based on an Instrument Container; Brenninkmeijer et
206 al., 2007) and MOZAIC (Measurements of OZone and water vapor by Airbus In-service
207 airCraft; Marenco et al., 1998) programs, providing measurements from ~60,000 flights since
208 1994. We note the relative lack of IAGOS data over the Pacific compared to the Atlantic (shorter
209 temporal record, lower flight frequency, and much fewer flights with concomitant O_3 and CO
210 measurements), and therefore limited the comparison to the Atlantic. Because commercial
211 aircraft cruise altitudes over the ocean are predominantly between 9 and 12 km, the comparison
212 between ATom and IAGOS is further limited to the UTLS (Fig. 1). More details are shown in
213 Table S1.
214 Identical dual-beam UV absorption photometers measured O_3 aboard the IAGOS flights.
215 An instrument comparison demonstrated that the photometers (standard model 49, Thermo
216 Scientific, modified for aircraft use) showed good consistency in measuring O_3 following an

inter-comparison experiment (Nédélec et al., 2015). The associated uncertainty is ± (2 ppbv + 2 %) at a 4-second sampling resolution (Thouret et al., 1998).

CO measurements were made using infra-red absorption photometers (standard model 48 Trace Level, Thermo Scientific, modified for aircraft use) with an uncertainty of ± (5 ppbv + 5 %) at a 30-second sampling resolution (Nédélec et al., 2003, 2015).

2.4 Ozonesondes

Ozonesondes have measured the vertical distribution of O_3 in the atmosphere for decades, and provide some of the longest tropospheric records that are commonly used to determine regional O_3 trends (Gaudel et al., 2018; Leonard et al., 2017; Oltmans et al., 2001; Tarasick et al., 2019a; Thompson et al., 2017). Ozonesonde launching sites are operated by the NOAA ESRL Global Monitoring Division (GMD), NASA Goddard's Southern Hemisphere Additional OZonesondes (SHADOZ) program, the New Zealand National Institute of Water & Atmospheric Research (NIWA), the National Meteorological Center of Argentina (SNMA) in collaboration with the Finnish Meteorological Institute (FMI), or Environment and Climate Change Canada. A more detailed description of each ozonesonde site and corresponding dataset can be found in Tables S1 and S2. All sites use electrochemical concentration cell (ECC) ozonesondes that rely on the potassium iodide electrochemical detection of O_3, and which provide a vertical resolution of about 100 m (Komhyr, 1969). The associated uncertainty is usually ± (5–10 %) (Tarasick et al., 2019b; Thompson et al., 2019; Witte et al., 2018).

2.5 Data analysis

In this analysis, ATom flight tracks were divided into the Atlantic and Pacific basins, and further subdivided into five regions within those basins: tropics, and northern and southern middle- and high-latitudes. Vertical profiles presented graphically in this paper show O_3 median values and the 25^{th} to 75^{th} percentile range within the 0–12 km tropospheric column sampled by the DC-8 aircraft. These medians were obtained by averaging with equal weight the individual profiles within each region over 1 km altitude bins.

HIPPO flight tracks are illustrated in Figure 1. The flight segments used for comparison with ATom were binned into the same Pacific latitude and longitude bands as for ATom. HIPPO vertical profile data are derived using the same methodology as for ATom.

All IAGOS flight tracks over the northern and tropical Atlantic are represented in Figure 1 in green. The latitude bands used to parse IAGOS data are consistent with the ones used for ATom. The longitude bands are 50° W to 20° W in the tropics, 50° W to 10° W in the northern midlatitudes, and 110° W to 10° W in the northern high-latitudes. Variations of the longitude band widths do not significantly affect the O_3 distributions measured by IAGOS. Data from all flights from 1994 to 2017 were included in the IAGOS dataset considered here, and were then divided into two altitude bins (8–10 km and 10–12 km) in order to better understand the influence of different O_3 sources (e.g., anthropogenic, stratospheric) on these two layers of the atmosphere.

We compare the ozonesonde measurements to ATom and HIPPO aircraft data sampled within 500 km of each ozonesonde launching site, since we expect a robust correlation in the free troposphere within this distance (Liu et al., 2009). We used the surface coordinates of the ozonesonde sites because the in-flight coordinates of ozonesondes are not available at all sites. For comparison with ozonesonde long term records, we consider three regions of the atmosphere: boundary layer (0–2 km), free troposphere (2–8 km), and UTLS (8–12 km). For each layer, we compared monthly O_3 distributions from ozonesondes with the corresponding seasonal O_3 distributions from aircraft measurements using the skill score (S_{score}) metric (Perkins et al., 2007). The S_{score} is calculated by summing the minimum probability of two normalized distributions at each bin center, and therefore measures the overlapping area between two probability distribution functions. If the distributions are identical, the skill score will equal 100 % (see Fig. S1 for further examples). Note the S_{score} is positively correlated with the size of the bin used to compare distributions. Here we chose a bin size of 5 ppbv, which is larger than the combined precision of ATom, HIPPO, and IAGOS measurements, but small enough to separate distinct air masses and their influence on O_3 distribution. Variables such as the distance to each ozonesonde launching site (500 km in this study), the bin size of the O_3 distributions (5 ppbv in this study), and the length of each ozonesonde record (full length in this study) can shift the vertically-averaged S_{score} value by up to 8 % (Table S3). We therefore treat this 8 % as a rough estimate of the precision of the S_{score} values presented here.

All three techniques (chemiluminescence, UV absorption, and ECC) used to measure O_3 for the datasets analyzed in this work have been shown to provide directly-comparable accurate measurements with well-defined uncertainties (Tarasick et al., 2019b).

279
280 2.6 Back trajectory analysis
281 Analysis of back trajectories for air masses sampled during airborne missions is useful to
282 examine the air mass source regions and causes for O_3 variability over the Pacific and Atlantic
283 Oceans. We calculated ten-day back trajectories using the Traj3D model (Bowman, 1993;
284 Bowman and Carrie, 2002) and National Centers for Environmental Prediction (NCEP) global
285 forecast system (GFS) meteorology. Trajectories were initialized each minute along all of the
286 ATom flight tracks.
287
288 **3. Comparison of ATom and HIPPO O_3 distributions to longer-term observational**
289 **records**
290 Here we use existing ozonesonde and IAGOS observations of O_3 at selected locations
291 along the ATom and HIPPO circuits to provide a climatological context for O_3 distributions
292 derived from the systematic airborne in situ "snapshots". We quantify how much of O_3
293 variability, occurring on timescales ranging from hours to decades, was captured by the
294 temporally-limited HIPPO and ATom missions.
295
296 3.1. Comparison to ozonesondes
297 ATom and HIPPO explored the fidelity with which airborne missions represent O_3
298 climatology in the remote troposphere. Here, we show that aircraft-measured median O_3 follows
299 the seasonal ozonesonde-measured median O_3 cycle at most of the sites studied here, and at
300 almost all altitudes – with a few exceptions (Figs. 2 and 3). Figure 2 plots the monthly median O_3
301 measurements from the tropical ozonesonde sites in three altitude bins, along with the median
302 values obtained from HIPPO and ATom measurements. Figure 3 plots the same for the
303 extratropical sites. Figure 4 correlates the median O_3 measured by aircraft in Figures 2 and 3
304 with those measured by ozonesondes. At the Eureka site, the winter and spring ATom
305 deployments recorded a significantly lower median O_3 compared to the corresponding
306 ozonesonde monthly median O_3 in the 0–2 km range (Fig. 3). Eureka is frequently subject to
307 springtime O_3 depletion events at the surface due to atmospheric bromine chemistry, which is
308 well recorded by the ozonesonde record (Fig. 3; Tarasick and Bottenheim, 2002). Sampling
309 during O_3 depletion events significantly lowered the ATom winter and springtime O_3

distributions near this site. In the 2–8 km range, there is a very good seasonal agreement between ATom/HIPPO and the ozonesondes (Fig. 4b). Most seasonal differences are found above 8 km (e.g., ATom in February at Trinidad Head and in May at Eureka; Fig. 3) and can be linked to the occurrence – or absence – of stratospheric air sampling during ATom and HIPPO. In the absence of stratospheric air mixing (< 8 km in Fig. 4), ATom/HIPPO successfully capture a large fraction of O_3 climatology everywhere (Figs. 4b and 4c).

Figures 5 and 6 show vertical profiles of O_3 distributions by season at each ozonesonde site, along with comparisons to HIPPO and ATom vertical profiles. Our analysis reveals that O_3 distributions derived from the ATom and HIPPO seasonal "snapshots" capture 30–71 % of the 1 km-vertically binned O_3 distribution established by long-term ozonesonde climatologies. For the nine ozonesonde sites considered here, ATom and HIPPO captured on average 53 %, 54 %, and 38 % of the O_3 distribution in the 0–2 km, 2–8 km, and 8–12 km altitude bins, respectively.

Larger differences between ATom/HIPPO and the ozonesonde records in the UTLS (8–12 km) can be ascribed to O_3 variability from stratospheric–tropospheric exchange, which is not always captured by the ATom and HIPPO missions. This increased O_3 variability in the UTLS is well-described by the long term ozonesonde records at Lauder, Trinidad Head, Eureka, Ushuaia, and Marambio (Figs. 3 and 6). In these middle- and high-latitude locations in both hemispheres, O_3 variability is especially pronounced during winter and spring, time periods favorable to more frequent stratospheric air mixing (Greenslade et al., 2017; Lin et al., 2015a; Tarasick et al., 2019a). Furthermore, the probability of sampling stratospheric air masses at ATom and HIPPO ceiling altitude (12–14 km) increases with latitude, resulting in a lower S_{score} between the ATom/HIPPO and ozonesonde datasets at the extra-tropical sites than at the tropical sites (Figs. S2a and S2b).

In the boundary layer (0–2 km) of the remote troposphere, O_3 variability is predominantly impacted by loss mechanisms. Ozonesonde records show instances of O_3 mixing ratios lower than 10 ppbv throughout the year in the boundary layer at the nine sites studied here (Figs. 2 and 3). The lowest O_3 mixing ratios are a result of (a) photochemical destruction over the oceans in the tropics (Monks et al., 1998, 2000; Thompson et al., 1993), (b) O_3-destroying halogen emissions in polar regions in springtime (e.g., Fan and Jacob, 1992), and (c) transport of O_3-poor oceanic air over the midlatitude sites (e.g., Neuman et al., 2012).

ATom and HIPPO best describe the O_3 distribution in the free troposphere (2–8 km; Figs. S2a and S2b). This suggests that airborne campaigns can capture global baseline O_3 values, along with the long-range transport of O_3 pollution plumes often lofted to this altitude range and responsible for O_3 variability.

While ATom consisted of one transect per ocean per season, HIPPO covered the Pacific twice per seasonal deployment (southbound and northbound). The 1 km-binned S_{score} is on average higher when two combined seasonal HIPPO flights (southbound and northbound) were available to compare to ozonesonde records, as opposed to when comparing O_3 profiles from individual HIPPO transects with ozonesonde records (Fig. S2c). In addition, two seasonal flights during HIPPO reduced the occurrence of low S_{score} values. This S_{score} decrease from flying only one Pacific transect only during ATom was traded for the increase of vertical profiles over the Atlantic Basin, which was not sampled during HIPPO. Future airborne missions with multiple seasonal vertical profiles over large-scale regions would be ideal to better depict the full range of tropospheric O_3 variability.

3.2. Comparison to IAGOS

IAGOS O_3 and CO observations in the northern Atlantic UTLS provide a measurement-based climatology at commercial aircraft cruise altitudes for comparison to ATom. Simultaneous measurements of O_3 and CO are of particular interest because CO provides a long-lived tracer of continental emissions, which helps to differentiate O_3 sources (Cohen et al., 2018). We note that while IAGOS measurements encompass hundreds of seasonal flights (depending on the region), ATom sampled within each latitude band and season on one or two flights only (Fig. 1). Thus, variability in the UT that occurred on timescales longer than a day was not captured by ATom. Consequently, it is not surprising to see that ATom systematically under-sampled tropospheric O_3 (and CO) variability compared to IAGOS at all latitudes in the northern Atlantic (Figs. 7 and 8). ATom captured on average 40 % of the O_3 variability measured by IAGOS in the Atlantic UTLS (Fig. 7), on par with the S_{score} of 38 % obtained when comparing ATom and HIPPO to ozonesonde data (see section 3.1).

In the middle- and high-latitudes, the shapes of the O_3 vs. CO scatterplots from IAGOS data demonstrate that distinct sources contribute to O_3 levels in the UTLS (Figs. 8a and 8b; Gaudel et al., 2015). The high O_3 (>150 ppbv) – low CO (<100 ppbv) range corresponds to intrusions of stratospheric air, which were mostly sampled in the spring season during ATom, supporting previous observations of increased stratospheric air mixing during this season (Lin et al., 2015a; Tarasick et al., 2019a). The low O_3 (<50 ppbv) – low CO (<100 ppbv) range corresponds to the tropospheric baseline air, whereas the intermediate O_3 (50–120 ppbv) – high CO (>100 ppbv) range generally represents the influence of air masses transported from continental regions. During ATom, high O_3 and low CO in the middle- and high-latitude UTLS were typical of stratospheric and baseline tropospheric air mixing.

O_3 measured during IAGOS rarely exceeds 150 ppbv in the northern tropical Atlantic UTLS (Fig. 8c). This is expected because the tropical tropopause is typically situated between 13 and 17 km altitude and IAGOS flights typically cruise below 12 km. Therefore, instances of stratospheric intrusions at IAGOS flight altitudes are limited. O_3 measured during ATom in the tropical Atlantic above 8 km was generally positively correlated with CO, showing the contribution of tropospheric O_3 production from continental sources reaching high altitudes. Given this variability, the ATom data do not capture the extrema of UTLS O_3 variability in the IAGOS measurements (Figs. 7 and 8). However, the most frequently measured O_3 and CO values from ATom overlap with the most frequently measured O_3 and CO values from IAGOS (contours in Fig. 8), suggesting that ATom captured the mode of the O_3 and CO distributions from IAGOS in the northern Atlantic UTLS.

4. O_3 distributions in the remote troposphere from ATom and HIPPO

We have established the fidelity of ATom and HIPPO O_3 data by comparison to measurement-based climatologies of tropospheric O_3 from well-established ozonesonde and commercial aircraft monitoring programs. In the following sections we exploit the systematic nature of the ATom and HIPPO vertical profiles to provide a global-scale picture of tropospheric O_3 distributions in the remote atmosphere. Figure 9 presents the altitudinal, latitudinal, and seasonal distribution of tropospheric O_3 during ATom and HIPPO. Higher O_3 was measured during ATom & HIPPO in the Northern Hemisphere (NH) than in the Southern Hemisphere

(SH), both in the Pacific and in the Atlantic. This distribution gradient has previously been shown by global O_3 mapping from modeling, satellite, and ozonesonde analyses (e.g., Hu et al., 2017; Liu et al., 2013). This finding holds true throughout the tropospheric column from 0 to 8 km, both in the middle- and high-latitudes (Fig. S3). In the midlatitudes below 8 km, median O_3 ranged between 25 and 45 ppbv in the SH, and between 35 and 65 ppbv in the NH. In the high latitudes below 8 km, median O_3 ranged between 30 and 45 ppbv in the SH, and between 40 and 75 ppbv in the NH. Notable features in the global O_3 distribution are discussed in more detail in the following sections. Figure 10 presents the vertically-resolved distribution of tropospheric O_3 from 0–12 km for the Atlantic (ATom in green) and for the pacific (ATom in pink, HIPPO in blue). S_{score} values resulting from the comparison of HIPPO and ATom Pacific distributions are shown with blue diamonds, and from the comparison of ATom Atlantic and Pacific distributions with pink squares. Figure 11 is derived from Figure 10 and gives the S_{score} values against altitude in the first panel, as well as the relative difference of median O_3 from 0 to 8 km in the second panel.

4.1. Tropics

Vertical distribution. O_3 is at a minimum in the tropical marine boundary layer (MBL), especially over the Pacific (Fig. 10a). The lowest measured O_3 in this region was 5.4 ppbv in May during ATom, and 3.5 ppbv in January during HIPPO. The tropical MBL is a net O_3 sink owing to very slow O_3 production rates – NO levels averaged 22 ± 12 pptv in the Pacific and Atlantic MBL during ATom – and rapid photochemical destruction rates of O_3 in a sunny, humid environment (Kley et al., 1996; Parrish et al., 2016; Thompson et al., 1993). Deep stratospheric intrusions into the Pacific MBL were not observed in ATom or HIPPO, in contrast to reports from previous studies (e.g., Cooper et al., 2005; Nath et al., 2016). In the tropics, marine convection within the intertropical convergence zone (ITCZ) is associated with relatively low O_3 values throughout the tropospheric column, with median O_3 mixing ratios less than 25 ppbv below 4 km altitude in the tropical Pacific (Fig. 10a; Oltmans et al., 2001). The relative difference between ATom Atlantic and Pacific median O_3 in the tropics below 8 km is consistently higher than a factor of 1.5, with an average S_{score} of 43 % (Figs. 10a and 11b). We ascribe this difference to O_3 production from biomass burning (BB) emissions in the continental regions surrounding the tropical Atlantic; back trajectories from the ATom flight tracks show the

tropical Atlantic is strongly affected by transport from BB source regions in both Africa and South America (Fig. S4; Jensen et al., 2012; Sauvage et al., 2006; Stauffer et al., 2018; Thompson et al., 2000). In addition, the positive correlation of O_3 enhancements with black carbon (Katich et al., 2018) and reactive nitrogen species (Thompson et al., personal communication) also indicate BB influence. Although ATom and HIPPO data show evidence for extensive and widespread BB influence on O_3 in the Pacific as well, O_3 mixing ratios are consistently more elevated throughout the tropospheric column in the Atlantic. One reason is closer proximity of the mid-ocean Atlantic flight tracks to O_3 precursor source regions. These findings confirm studies that previously highlighted the impact of African BB emissions on O_3 production in the tropical Atlantic (e.g., Andreae et al., 1994; Fishman et al., 1996; Jourdain et al., 2007; Williams et al., 2010). Lightning NO_x also play a role in the buildup of O_3 over the tropical Atlantic at certain times of year (Moxim and Levy, 2000; Pickering et al., 1996).

Seasonality. The seasonal variation of vertical profiles of O_3 in the tropics is lower throughout the column compared to the extra-tropics (Fig. 12), in part due to less stratospheric influence at the highest tropical altitudes. The remoteness of the tropical Pacific flight paths from continental pollution sources also drives the lower seasonal variability here compared to the tropical Atlantic, where BB influence peaks in June–August and October–November, characterized by high O_3 (> 75 ppbv) and high CO (>100 ppbv) (Fig. 13f), significantly increasing the O_3 vertical distribution compared to the other seasons (Figs. 12c, 12h, and 12m). Finally, photochemistry, which regulates O_3 net balance in the troposphere, is less seasonally variable in the tropics than in the extra-tropics, where the photolysis frequency of O_3 ($j(O_3)$) and photochemical production of O_3 fluctuate annually with solar zenith angle.

O_3 minima and maxima. Coincident O_3 and CO enhancements were observed in the tropical Atlantic for each ATom circuit (Figs. 9 and 13f), suggesting a year-round influence of continental emissions and distinctive dynamics in this region (Krishnamurti et al., 1996; Thompson et al., 1996). In the tropical Pacific, the April–May period stands out due to an O_3 and CO enhancement episode during HIPPO (Fig. 9) that was attributed to the transport of anthropogenic and BB emissions from southeast Asia (Shen et al., 2014). Deep convection in the tropics brings O_3-poor (<15 ppbv) air to the upper troposphere (Kley et al., 1996; Pan et al., 2015; Solomon et al., 2005). However, the spatial extent of these events remains poorly constrained. Results from ATom and HIPPO suggest that deep convection can loft O_3-poor air at

464 least up to 12 km (the altitude ceiling of this study) in the tropical Pacific, and occurred more
465 frequently between January and May (Figs. 12c and h). During the rest of the year, O_3-poor air
466 was typically confined below 4 km. Conversely, O_3-poor air is confined to the first 2 km in the
467 tropical Atlantic (Fig. S5). Meteorological analysis of tropical ozonesondes shows that
468 subsidence of higher-O_3 air aloft over the Atlantic is one reason O_3-poor air is found only in the
469 boundary layer (Thompson et al., 2000, 2012).
470
471 4.2. Middle- and high-latitudes
472 **Vertical distribution.** In the middle- and high-latitudes, tropospheric O_3 was generally at
473 a minimum in the MBL and increased with altitude. Above 8 km, increasing O_3 with altitude
474 (Figs. 10b–e) and its persistent anticorrelation with CO (Fig. 13) points to stratospheric air
475 sampling as the cause for higher O_3 variability in the extra-tropical UTLS, especially at high
476 latitudes where the tropopause is lower and wave breaking of the polar jet streams can lead to
477 stratospheric intrusions. As a result, the S_{score} decrease above 8 km, summarized in Figure 11a, is
478 ascribed to variability in the influence of stratospheric air. ATom detected little change in the O_3
479 distribution over the Pacific Ocean since HIPPO, with a S_{score} averaging 74 % in the 0–8 km
480 range. The relative difference between median O_3 values from HIPPO and ATom in the Pacific
481 is generally lower than 20 % (Fig. 11b). Similarly, the relative difference between median O_3
482 mixing ratios between ATom Atlantic and Pacific below 8 km is consistently lower than 20 %,
483 with an average S_{score} of 75 % (Fig. 11b). The southern high-latitudes are the only region where
484 the S_{score} below 8 km occasionally fell below 60 % (Fig. 10e). However, a lower S_{score} was
485 expected there as the Atlantic vertical profile is based on only two seasonal flights to Antarctica,
486 whereas there were four seasonal flights in the Pacific. Additionally, HIPPO was less spatially
487 extensive – resulting in fewer data points – in this latitude bin compared to ATom (Fig. 1), which
488 could explain the low S_{score} values when comparing the two missions (Fig. 10e). Nevertheless,
489 the similar O_3 distribution in the extra-tropical free troposphere above the two oceans is
490 consistent with an O_3 lifetime sufficiently long for rapid zonal transport to smooth out variations
491 in baseline O_3 distribution in the remote troposphere, across a relatively wide range of longitudes
492 (Figs. 10b–e). The comparison of O_3 seasonal cycles at remote ozonesonde launching sites of the
493 northern midlatitudes yields similar results and further supports this conclusion (Logan, 1985;
494 Parrish et al., 2020). However, the similarity of the O_3 distribution in the extra-tropical free

troposphere above the Atlantic and Pacific is not always evident in satellite-, modelling-, or ozonesonde-derived maps (Gaudel et al., 2018; Hu et al., 2017; Ziemke et al., 2017). Additionally, studies of the spatial representativeness of tropospheric O_3 monitoring networks have also concluded that tropospheric O_3 distributions varied significantly with longitude, especially in the northern middle- and high-latitudes over continents (Liu et al., 2013; Tilmes et al., 2012). In contrast, the ATom findings stem from O_3 measurements predominantly over the oceans, which likely reveal a different picture of O_3 longitudinal distribution away from regional precursor emissions.

Seasonality. The extra-tropical vertical profiles of O_3 vary seasonally during ATom and HIPPO. The summer season in the middle- and high-latitudes was remarkable over both oceans and hemispheres for the steep O_3 gradients in the tropospheric column (Fig. 12 in black). In the MBL, median O_3 was consistently under 25 ppbv in the summer, whereas O_3 was over 25 ppbv in other seasons. Low O_3 in the MBL in summer reflects the enhanced O_3 photochemical destruction in this NO_x-limited region. Photochemical destruction decreases in dry air in the upper troposphere, thus leading to the steep O_3 gradients observed here. The summer O_3 minimum was especially apparent in the high latitudes of the southern Pacific during ATom and extended well above the MBL into the free troposphere (Fig. 12 in black). O_3 mixing ratios were highest in the tropospheric column during springtime in both hemispheres, and over both oceans (Fig. 12 in gold). A notable exception occurred during springtime in the high latitudes of the NH, where several O_3 depletion events were sampled in the lower legs of the Arctic transit. During these events, O_3 mixing ratios lower than 10 ppbv were measured, resulting in a lower 25th percentile of O_3 distribution at the lowest altitude compared to the other seasons (Figs. 12e and 12o in gold). A tropospheric O_3 springtime maximum has often been reported in the NH (e.g., Monks, 2000) when meteorology favors efficient transport of O_3 and precursors from continental air from North America and Eurasia (Owen et al., 2006; Zhang et al., 2017, 2008). Another contributing factor is the increased frequency of stratospheric air mixing in spring that significantly contributes to higher O_3 levels (Lin et al., 2015a; Tarasick et al., 2019a). Further, the tropospheric O_3 springtime maximum in the SH is often attributed to BB emissions reaching a peak (Fishman et al., 1991; Gaudel et al., 2018), but stratospheric air mixing also occurs (Diab et al., 1996, 2004; Greenslade et al., 2017). Here, the O_3/CO relationship in spring shows that the enhanced stratospheric mixing with tropospheric air during this season, both in the northern and

526 southern middle- and high-latitudes, contributes to the increase in column O_3 (Fig. 13). Fall and
527 winter seasons shared similar features in the middle- and high-latitudes: no strong O_3 gradient
528 was measured in the free troposphere, and O_3 values varied over similar ranges – about 40 ppbv
529 in the NH and about 30 ppbv in the SH – during the two seasons (Fig. 12 in red and blue).
530 **O_3 enhancements.** The linear increase of O_3 with CO >100 ppbv highlights the
531 contribution of natural and anthropogenic pollution plumes lofted from continental areas into the
532 remote troposphere. In the NH, these events occur almost year-round (Figs. 13b–c and 13g–h).
533 Higher CO enhancements in the Pacific (Figs. 13g–h) than in the Atlantic (Figs. 13b–c) have
534 been observed before and attributed to sampling bias (Clark et al., 2015). Here, our findings
535 suggest a year-round influence of continental emissions on the Pacific atmosphere despite its
536 remoteness. Modeled back trajectories show that most air masses sampled in the NH during
537 ATom were influenced by long-range transport of continental emissions from Asia, Africa, and
538 North America (Fig. S6). Previous studies have shown anthropogenic and BB emission outflow
539 from Asia significantly contributed to O_3 pollution events measured over the northern Pacific or
540 in California (e.g., Heald et al., 2003; Jaffe et al., 2004; Lin et al., 2017). Intercontinental
541 transport of anthropogenic emissions from Europe can also contribute to the Asian outflow of
542 anthropogenic pollution (e.g., Bey et al., 2001; Liu et al., 2002; Newell and Evans, 2000).
543 Finally, O_3 enhancements in the northern Atlantic were frequently observed and attributed to
544 midlatitude anthropogenic and boreal forest fire emissions (e.g., Honrath et al., 2004; Martín et
545 al., 2006; Trickl et al., 2003). In the SH, polluted air is encountered more often in spring and
546 summer over the Atlantic, but springtime CO is greater than in other seasons over the Pacific
547 (Figs. 13d–e and 13i–j). During spring, median O_3 above 50 ppbv was measured throughout the
548 free troposphere in the southern midlatitudes (Fig. 12). Several air masses intercepted during
549 these flights originated from regions that were intensively burning at the time, notably equatorial
550 and southern Africa, Australia, and southern South America, contributing to the observed
551 enhanced O_3 and CO (Fig. S4). Our results expand on previous observation-based, but more
552 spatially and temporally limited, studies that highlighted collocated enhancements of O_3 and CO
553 at remote locations to show in situ evidence of frequent, large-scale influence of continental
554 outflow on O_3 in the remote troposphere in both oceans, and at almost all latitudes.
555
556 **5. Conclusion**

We present tropospheric O_3 distributions measured over remote regions of the Pacific and Atlantic Oceans during two airborne chemical sampling projects: the four deployments of ATom (2016–2018) and the five deployments of HIPPO (2009–2011). The data highlight several regional- and large-scale features of O_3 distributions, and provide insight into current O_3 distributions in remote regions. The main findings are as follows:

- ATom and HIPPO provide a unique perspective on vertically-resolved global baseline O_3 distributions over the Pacific and Atlantic basins, and expand upon spatially-limited O_3 climatologies from long-term datasets to highlight large-scale features necessary for model output and satellite retrieval validation.
- ATom and HIPPO O_3 data are consistent – where they overlap – with measurement-based climatologies of tropospheric O_3 from well-established ozonesonde and commercial aircraft monitoring programs. ATom and HIPPO seasonal median O_3 correlated well with corresponding seasonal median O_3 from ozonesondes ($R^2 > 0.7$), giving confidence in the accurate depiction of the emerging global O_3 climatology by these diverse research activities. ATom and HIPPO captured 30–71 % of O_3 variability measured by ozonesondes launched in the vicinity of the aircraft flight tracks, and had the same mode of the O_3 distribution as determined by IAGOS in the northern Atlantic UTLS. This representativeness evaluation on global scales highlights the usefulness of airborne observations to fill in the gaps of established but limited O_3 climatologies. Higher O_3 loading in the NH compared to the SH is consistent with the heterogeneous distribution of O_3 precursor emissions around the globe, mostly concentrated in the NH, a result consistent with previous modeling studies and satellite observations. ATom Atlantic vs. Pacific comparison reveals a similar O_3 distribution in the free troposphere up to ~8 km in the middle- and high-latitudes, but not in the tropics. Similar O_3 distributions across latitude bands have been suggested in the past, but these studies were limited to the northern midlatitudes. Conversely, other satellite, modeling, and observation-based studies indicated significant O_3 longitudinal gradients. Here, our findings are consistent with zonal transport smoothing the baseline O_3 distribution longitudinally from the Pacific to the Atlantic. In the tropics, median O_3 mixing ratios are about twice as high in the Atlantic than in the Pacific, due to a well-documented mixture of dynamical patterns interacting with the transport of continental air masses.

- A comparison of seasonal O_3 vertical profiles did not reveal a marked seasonality in the tropics, but instead highlighted the influence of specific events, most notably BB emissions from Africa and South America, which have been extensively documented in the literature. In the extra-tropics, the summer season was characterized by a steeper tropospheric O_3 gradient driven by very low O_3 abundance in the MBL. Fall and winter seasons generally led to near-constant O_3 mixing ratios from the surface to the upper troposphere, while the highest O_3 abundance was recorded during the spring season when more frequent and intense stratospheric intrusions and transport of air masses from continental regions occur. ATom and HIPPO provide the first airborne in situ vertically-resolved O_3 climatology covering both the Atlantic and Pacific Oceans in the NH and in the SH. They confirm and extend the current understanding of O_3 variability in the remote troposphere, built over several decades by airborne campaigns, monitoring networks, and satellite observations.
- Overall, this paper highlights the value of the ATom and HIPPO datasets, which cover spatial scales commensurate with the grid resolution of current Earth system models, and further, are useful as a priori estimates for improved retrievals of tropospheric O_3 from satellite remote sensing platforms. In addition, ATom and HIPPO in situ measurements help to establish the quantitative legacy of global pollution transport and chemistry through the evaluation of key, covarying species – in this case O_3 and CO, and reveal the year-round pervasive influence of continental outflow on O_3 enhancements in the remote troposphere. ATom and HIPPO datasets should be critical for improving the scientific community's understanding of O_3 production and loss processes, and the influence of anthropogenic emissions on baseline O_3 in remote regions. They provide a timely addition to the Tropospheric Ozone Assessment Report (TOAR) effort to characterize the global-scale O_3 distribution, and address some of the measurement gaps identified therein.

Author Contribution

SCW and TBR designed the research (ATom and HIPPO). The measurements were done by IB, JP, CRT, TC, RC, BD, GWD, JWE, RSG, EJH, KM, FLM, CS, and TBR. BJJ, RK, RQ, RS, DWT, AMT, and JCW provided the ozonesonde measurements. HC, AG, and VT provided the

IAGOS measurements. Back trajectory calculations were provided by ER and KCA. IB, JP, CRT, KCA, RC, AG, EJH, KM, DDP, RQ, ER, DWT, AMT, VT, JCW, SCW, and TBR contributed to the discussion and interpretation of the results. IB, JP, and TBR wrote the paper.

Competing interests

The authors declare no competing interest.

Acknowledgments

We thank the ATom leadership team, science team, and DC-8 pilots and crew for contributions to the ATom measurements. ATom was funded in response to NASA ROSES-2013 NRA NNH13ZDA001N-EVS2. The authors acknowledge support by the U.S. National Oceanic and Atmospheric Administration (NOAA) Health of the Atmosphere and Atmospheric Chemistry, Carbon Cycle, and Climate Programs. SHADOZ ozonesondes are supported by the Upper Atmosphere Research Program of NASA. Ozonesoundings at Marambio have been supported by the Finnish Antarctic research program (FINNARP). The IAGOS program acknowledges the European Commission for its support of the MOZAIC project (1994-2003) the preparatory phase of IAGOS (2005-2013) and IGAS (2013-2016); the partner institutions of the IAGOS Research Infrastructure (FZJ, DLR, MPI, KIT in Germany, CNRS, Météo-France, Université Paul Sabatier in France, and University of Manchester, UK); the French Atmospheric Data Center AERIS for hosting the database; and the participating airlines (Lufthansa, Air France, China Airlines, Iberia, Cathay Pacific, Hawaiian Airlines) for transporting the instrumentation free of charge. We thank J. A. Neuman, H. Angot, and O. Cooper for helpful discussions and careful editing of this manuscript.

References

Andreae, M. O., Anderson, B. E., Blake, D. R., Bradshaw, J. D., Collins, J. E., Gregory, G. L., Sachse, G. W. and Shipham, M. C.: Influence of plumes from biomass burning on atmospheric chemistry over the equatorial and tropical South Atlantic during CITE 3, Journal of Geophysical Research, 99(D6), 12793, doi:10.1029/94JD00263, 1994.

649 Bey, I., Jacob, D. J., Logan, J. A. and Yantosca, R. M.: Asian chemical outflow to the Pacific in
650 spring: Origins, pathways, and budgets, Journal of Geophysical Research: Atmospheres,
651 106(D19), 23097–23113, doi:10.1029/2001JD000806, 2001.

652 Bowman, K. P.: Large-scale isentropic mixing properties of the Antarctic polar vortex from
653 analyzed winds, Journal of Geophysical Research: Atmospheres, 98(D12), 23013–23027,
654 doi:10.1029/93JD02599, 1993.

655 Bowman, K. P. and Carrie, G. D.: The Mean-Meridional Transport Circulation of the Troposphere
656 in an Idealized GCM, J. Atmos. Sci., 59(9), 1502–1514, doi:10.1175/1520-
657 0469(2002)059<1502:TMMTCO>2.0.CO;2, 2002.

658 Brenninkmeijer, C. a. M., Crutzen, P., Boumard, F., Dauer, T., Dix, B., Ebinghaus, R., Filippi, D.,
659 Fischer, H., Franke, H., Frieβ, U., Heintzenberg, J., Helleis, F., Hermann, M., Kock, H. H., Koeppel,
660 C., Lelieveld, J., Leuenberger, M., Martinsson, B. G., Miemczyk, S., Moret, H. P., Nguyen, H. N.,
661 Nyfeler, P., Oram, D., O'Sullivan, D., Penkett, S., Platt, U., Pupek, M., Ramonet, M., Randa, B.,
662 Reichelt, M., Rhee, T. S., Rohwer, J., Rosenfeld, K., Scharffe, D., Schlager, H., Schumann, U.,
663 Slemr, F., Sprung, D., Stock, P., Thaler, R., Valentino, F., Velthoven, P. van, Waibel, A., Wandel,
664 A., Waschitschek, K., Wiedensohler, A., Xueref-Remy, I., Zahn, A., Zech, U. and Ziereis, H.: Civil
665 Aircraft for the regular investigation of the atmosphere based on an instrumented container:
666 The new CARIBIC system, Atmospheric Chemistry and Physics, 7(18), 4953–4976,
667 doi:https://doi.org/10.5194/acp-7-4953-2007, 2007.

668 Browell, E. V., Fenn, M. A., Butler, C. F., Grant, W. B., Merrill, J. T., Newell, R. E., Bradshaw, J. D.,
669 Sandholm, S. T., Anderson, B. E., Bandy, A. R., Bachmeier, A. S., Blake, D. R., Davis, D. D.,
670 Gregory, G. L., Heikes, B. G., Kondo, Y., Liu, S. C., Rowland, F. S., Sachse, G. W., Singh, H. B.,
671 Talbot, R. W. and Thornton, D. C.: Large-scale air mass characteristics observed over western
672 Pacific during summertime, Journal of Geophysical Research: Atmospheres, 101(D1), 1691–
673 1712, doi:10.1029/95JD02200, 1996a.

674 Browell, E. V., Fenn, M. A., Butler, C. F., Grant, W. B., Clayton, M. B., Fishman, J., Bachmeier, A.
675 S., Anderson, B. E., Gregory, G. L., Fuelberg, H. E., Bradshaw, J. D., Sandholm, S. T., Blake, D. R.,
676 Heikes, B. G., Sachse, G. W., Singh, H. B. and Talbot, R. W.: Ozone and aerosol distributions and
677 air mass characteristics over the South Atlantic Basin during the burning season, Journal of
678 Geophysical Research: Atmospheres, 101(D19), 24043–24068, doi:10.1029/95JD02536, 1996b.

679 Clark, H., Sauvage, B., Thouret, V., Nédélec, P., Blot, R., Wang, K.-Y., Smit, H., Neis, P., Petzold,
680 A., Athier, G., Boulanger, D., Cousin, J.-M., Beswick, K., Gallagher, M., Baumgardner, D., Kaiser,
681 J., Flaud, J.-M., Wahner, A., Volz-Thomas, A. and Cammas, J.-P.: The first regular measurements
682 of ozone, carbon monoxide and water vapour in the Pacific UTLS by IAGOS, Tellus B: Chemical
683 and Physical Meteorology, 67(1), 28385, doi:10.3402/tellusb.v67.28385, 2015.

684 Cohen, Y., Petetin, H., Thouret, V., Marécal, V., Josse, B., Clark, H., Sauvage, B., Fontaine, A.,
685 Athier, G., Blot, R., Boulanger, D., Cousin, J.-M. and Nédélec, P.: Climatology and long-term
686 evolution of ozone and carbon monoxide in the upper troposphere–lower stratosphere (UTLS)

687 at northern midlatitudes, as seen by IAGOS from 1995 to 2013, Atmospheric Chemistry and
688 Physics, 18(8), 5415–5453, doi:https://doi.org/10.5194/acp-18-5415-2018, 2018.

689 Cooper, O. R., Stohl, A., Hübler, G., Hsie, E. Y., Parrish, D. D., Tuck, A. F., Kiladis, G. N., Oltmans,
690 S. J., Johnson, B. J., Shapiro, M., Moody, J. L. and Lefohn, A. S.: Direct transport of midlatitude
691 stratospheric ozone into the lower troposphere and marine boundary layer of the tropical
692 Pacific Ocean, J. Geophys. Res., 110(D23), D23310, doi:10.1029/2005JD005783, 2005.

693 Cooper, O. R., Parrish, D. D., Ziemke, J., Balashov, N. V., Cupeiro, M., Galbally, I. E., Gilge, S.,
694 Horowitz, L., Jensen, N. R., Lamarque, J.-F., Naik, V., Oltmans, S. J., Schwab, J., Shindell, D. T.,
695 Thompson, A. M., Thouret, V., Wang, Y. and Zbinden, R. M.: Global distribution and trends of
696 tropospheric ozone: An observation-based review, Elem Sci Anth, 2(0),
697 doi:10.12952/journal.elementa.000029, 2014.

698 Crawford, J., Davis, D., Chen, G., Bradshaw, J., Sandholm, S., Kondo, Y., Liu, S., Browell, E.,
699 Gregory, G., Anderson, B., Sachse, G., Collins, J., Barrick, J., Blake, D., Talbot, R. and Singh, H.: An
700 assessment of ozone photochemistry in the extratropical western North Pacific: Impact of
701 continental outflow during the late winter/early spring, Journal of Geophysical Research:
702 Atmospheres, 102(D23), 28469–28487, doi:10.1029/97JD02600@10.1002/(ISSN)2169-
703 8996.PEMWEST1, 1997.

704 Crutzen, P. J.: Photochemical reactions initiated by and influencing ozone in unpolluted
705 tropospheric air, Tellus, 26(1–2), 47–57, doi:10.3402/tellusa.v26i1-2.9736, 1974.

706 Davis, D. D., Crawford, J., Chen, G., Chameides, W., Liu, S., Bradshaw, J., Sandholm, S., Sachse,
707 G., Gregory, G., Anderson, B., Barrick, J., Bachmeier, A., Collins, J., Browell, E., Blake, D.,
708 Rowland, S., Kondo, Y., Singh, H., Talbot, R., Heikes, B., Merrill, J., Rodriguez, J. and Newell, R.
709 E.: Assessment of ozone photochemistry in the western North Pacific as inferred from PEM-
710 West A observations during the fall 1991, Journal of Geophysical Research: Atmospheres,
711 101(D1), 2111–2134, doi:10.1029/95JD02755, 1996.

712 Derwent, R. G., Parrish, D. D., Galbally, I. E., Stevenson, D. S., Doherty, R. M., Young, P. J. and
713 Shallcross, D. E.: Interhemispheric differences in seasonal cycles of tropospheric ozone in the
714 marine boundary layer: Observation-model comparisons, Journal of Geophysical Research:
715 Atmospheres, 121(18), 11,075-11,085, doi:10.1002/2016JD024836, 2016.

716 Diab, R. D., Thompson, A. M., Zunckel, M., Coetzee, G. J. R., Combrink, J., Bodeker, G. E.,
717 Fishman, J., Sokolic, F., McNamara, D. P., Archer, C. B. and Nganga, D.: Vertical ozone
718 distribution over southern Africa and adjacent oceans during SAFARI-92, Journal of Geophysical
719 Research: Atmospheres, 101(D19), 23823–23833, doi:10.1029/96JD01267, 1996.

720 Diab, R. D., Thompson, A. M., Mari, K., Ramsay, L. and Coetzee, G. J. R.: Tropospheric ozone
721 climatology over Irene, South Africa, from 1990 to 1994 and 1998 to 2002, Journal of
722 Geophysical Research: Atmospheres, 109(D20), doi:10.1029/2004JD004793, 2004.

723 Edwards, D. P., Lamarque, J.-F., Attié, J.-L., Emmons, L. K., Richter, A., Cammas, J.-P., Gille, J. C.,
724 Francis, G. L., Deeter, M. N., Warner, J., Ziskin, D. C., Lyjak, L. V., Drummond, J. R. and Burrows,
725 J. P.: Tropospheric ozone over the tropical Atlantic: A satellite perspective, Journal of
726 Geophysical Research: Atmospheres, 108(D8), doi:10.1029/2002JD002927, 2003.

727 Fan, S.-M. and Jacob, D. J.: Surface ozone depletion in Arctic spring sustained by bromine
728 reactions on aerosols, Nature, 359(6395), 522–524, doi:10.1038/359522a0, 1992.

729 Fenn, M. A., Browell, E. V., Butler, C. F., Grant, W. B., Kooi, S. A., Clayton, M. B., Gregory, G. L.,
730 Newell, R. E., Zhu, Y., Dibb, J. E., Fuelberg, H. E., Anderson, B. E., Bandy, A. R., Blake, D. R.,
731 Bradshaw, J. D., Heikes, B. G., Sachse, G. W., Sandholm, S. T., Singh, H. B., Talbot, R. W. and
732 Thornton, D. C.: Ozone and aerosol distributions and air mass characteristics over the South
733 Pacific during the burning season, Journal of Geophysical Research: Atmospheres, 104(D13),
734 16197–16212, doi:10.1029/1999JD900065, 1999.

735 Fishman, J., Watson, C. E., Larsen, J. C. and Logan, J. A.: Distribution of tropospheric ozone
736 determined from satellite data, Journal of Geophysical Research: Atmospheres, 95(D4), 3599–
737 3617, doi:10.1029/JD095iD04p03599, 1990.

738 Fishman, J., Fakhruzzaman, K., Cros, B. and Nganga, D.: Identification of Widespread Pollution in
739 the Southern Hemisphere Deduced from Satellite Analyses, Science, 252(5013), 1693–1696,
740 doi:10.1126/science.252.5013.1693, 1991.

741 Fishman, J., Hoell, J. M., Bendura, R. D., McNeal, R. J. and Kirchhoff, V. W. J. H.: NASA GTE
742 TRACE A experiment (September–October 1992): Overview, Journal of Geophysical Research:
743 Atmospheres, 101(D19), 23865–23879, doi:10.1029/96JD00123, 1996.

744 Gaudel, A., Clark, H., Thouret, V., Jones, L., Inness, A., Flemming, J., Stein, O., Huijnen, V., Eskes,
745 H., Nedelec, P. and Boulanger, D.: On the use of MOZAIC-IAGOS data to assess the ability of the
746 MACC reanalysis to reproduce the distribution of ozone and CO in the UTLS over Europe, Tellus
747 B: Chemical and Physical Meteorology, 68(s1), 27955, doi:10.3402/tellusb.v67.27955, 2015.

748 Gaudel, A., Cooper, O. R., Ancellet, G., Barret, B., Boynard, A., Burrows, J. P., Clerbaux, C.,
749 Coheur, P.-F., Cuesta, J., Cuevas, E., Doniki, S., Dufour, G., Ebojie, F., Foret, G., Garcia, O.,
750 Muños, M. J. G., Hannigan, J. W., Hase, F., Huang, G., Hassler, B., Hurtmans, D., Jaffe, D., Jones,
751 N., Kalabokas, P., Kerridge, B., Kulawik, S. S., Latter, B., Leblanc, T., Flochmoën, E. L., Lin, W., Liu,
752 J., Liu, X., Mahieu, E., McClure-Begley, A., Neu, J. L., Osman, M., Palm, M., Petetin, H.,
753 Petropavlovskikh, I., Querel, R., Rahpoe, N., Rozanov, A., Schultz, M. G., Schwab, J., Siddans, R.,
754 Smale, D., Steinbacher, M., Tanimoto, H., Tarasick, D. W., Thouret, V., Thompson, A. M., Trickl,
755 T., Weatherhead, E., Wespes, C., Worden, H. M., Vigouroux, C., Xu, X., Zeng, G. and Ziemke, J.:
756 Tropospheric Ozone Assessment Report: Present-day distribution and trends of tropospheric
757 ozone relevant to climate and global atmospheric chemistry model evaluation, Elem Sci Anth,
758 6(1), doi:10.1525/elementa.291, 2018.

759 Greenslade, J. W., Alexander, S. P., Schofield, R., Fisher, J. A. and Klekociuk, A. K.: Stratospheric
760 ozone intrusion events and their impacts on tropospheric ozone in the Southern Hemisphere,
761 Atmospheric Chemistry and Physics, 17(17), 10269–10290, doi:10.5194/acp-17-10269-2017,
762 2017.

763 Heald, C. L., Jacob, D. J., Fiore, A. M., Emmons, L. K., Gille, J. C., Deeter, M. N., Warner, J.,
764 Edwards, D. P., Crawford, J. H., Hamlin, A. J., Sachse, G. W., Browell, E. V., Avery, M. A., Vay, S.
765 A., Westberg, D. J., Blake, D. R., Singh, H. B., Sandholm, S. T., Talbot, R. W. and Fuelberg, H. E.:
766 Asian outflow and trans-Pacific transport of carbon monoxide and ozone pollution: An
767 integrated satellite, aircraft, and model perspective, Journal of Geophysical Research:
768 Atmospheres, 108(D24), doi:10.1029/2003JD003507, 2003.

769 Holmes, C. D., Prather, M. J., Søvde, O. A. and Myhre, G.: Future methane, hydroxyl, and their
770 uncertainties: key climate and emission parameters for future predictions, Atmos. Chem. Phys.,
771 13(1), 285–302, doi:10.5194/acp-13-285-2013, 2013.

772 Honrath, R. E., Owen, R. C., Martín, M. V., Reid, J. S., Lapina, K., Fialho, P., Dziobak, M. P., Kleissl,
773 J. and Westphal, D. L.: Regional and hemispheric impacts of anthropogenic and biomass burning
774 emissions on summertime CO and O3 in the North Atlantic lower free troposphere, Journal of
775 Geophysical Research: Atmospheres, 109(D24), doi:10.1029/2004JD005147, 2004.

776 Hu, L., Jacob, D. J., Liu, X., Zhang, Y., Zhang, L., Kim, P. S., Sulprizio, M. P. and Yantosca, R. M.:
777 Global budget of tropospheric ozone: Evaluating recent model advances with satellite (OMI),
778 aircraft (IAGOS), and ozonesonde observations, Atmospheric Environment, 167, 323–334,
779 doi:10.1016/j.atmosenv.2017.08.036, 2017.

780 IPCC: Climate Change 2013: The Physical Science Basis. Contribution of Working Group I to the
781 Fifth Assessment Report of the Intergovernmental Panel on Climate Change, Cambridge
782 University Press, Cambridge, United Kingdom and New York, NY, USA. [online] Available from:
783 https://www.ipcc.ch/report/ar5/wg1/ (Accessed 8 January 2019), 2013.

784 Jacob, D. J., Heikes, E. G., Fan, S.-M., Logan, J. A., Mauzerall, D. L., Bradshaw, J. D., Singh, H. B.,
785 Gregory, G. L., Talbot, R. W., Blake, D. R. and Sachse, G. W.: Origin of ozone and NOx in the
786 tropical troposphere: A photochemical analysis of aircraft observations over the South Atlantic
787 basin, Journal of Geophysical Research: Atmospheres, 101(D19), 24235–24250,
788 doi:10.1029/96JD00336, 1996.

789 Jaffe, D., Bertschi, I., Jaeglé, L., Novelli, P., Reid, J. S., Tanimoto, H., Vingarzan, R. and Westphal,
790 D. L.: Long-range transport of Siberian biomass burning emissions and impact on surface ozone
791 in western North America, Geophysical Research Letters, 31(16), doi:10.1029/2004GL020093,
792 2004.

793 Jensen, A. A., Thompson, A. M. and Schmidlin, F. J.: Classification of Ascension Island and Natal
794 ozonesondes using self-organizing maps, Journal of Geophysical Research: Atmospheres,
795 117(D4), doi:10.1029/2011JD016573, 2012.

Jourdain, L., Worden, H. M., Worden, J. R., Bowman, K., Li, Q., Eldering, A., Kulawik, S. S., Osterman, G., Boersma, K. F., Fisher, B., Rinsland, C. P., Beer, R. and Gunson, M.: Tropospheric vertical distribution of tropical Atlantic ozone observed by TES during the northern African biomass burning season, Geophysical Research Letters, 34(4), doi:10.1029/2006GL028284, 2007.

Junge, C. E.: Global ozone budget and exchange between stratosphere and troposphere, Tellus, 14(4), 363–377, doi:10.1111/j.2153-3490.1962.tb01349.x, 1962.

Katich, J. M., Samset, B. H., Bui, T. P., Dollner, M., Froyd, K. D., Campuzano-Jost, P., Nault, B. A., Schroder, J. C., Weinzierl, B. and Schwarz, J. P.: Strong Contrast in Remote Black Carbon Aerosol Loadings Between the Atlantic and Pacific Basins, Journal of Geophysical Research: Atmospheres, 123(23), 13,386-13,395, doi:10.1029/2018JD029206, 2018.

Kley, D., Crutzen, P. J., Smit, H. G. J., Vömel, H., Oltmans, S. J., Grassl, H. and Ramanathan, V.: Observations of Near-Zero Ozone Concentrations Over the Convective Pacific: Effects on Air Chemistry, Science, 274(5285), 230–233, doi:10.1126/science.274.5285.230, 1996.

Komhyr, W.: Electrochemical Concentration Cells for Gas Analysis, Annales De Geophysique, 25(1), 203-, 1969.

Kondo, Y., Morino, Y., Takegawa, N., Koike, M., Kita, K., Miyazaki, Y., Sachse, G. W., Vay, S. A., Avery, M. A., Flocke, F., Weinheimer, A. J., Eisele, F. L., Zondlo, M. A., Weber, R. J., Singh, H. B., Chen, G., Crawford, J., Blake, D. R., Fuelberg, H. E., Clarke, A. D., Talbot, R. W., Sandholm, S. T., Browell, E. V., Streets, D. G. and Liley, B.: Impacts of biomass burning in Southeast Asia on ozone and reactive nitrogen over the western Pacific in spring, Journal of Geophysical Research: Atmospheres, 109(D15), doi:10.1029/2003JD004203, 2004.

Krishnamurti, T. N., Sinha, M. C., Kanamitsu, M., Oosterhof, D., Fuelberg, H., Chatfield, R., Jacob, D. J. and Logan, J.: Passive tracer transport relevant to the TRACE A experiment, Journal of Geophysical Research: Atmospheres, 101(D19), 23889–23907, doi:10.1029/95JD02419, 1996.

Leonard, M., Petropavlovskikh, I., Lin, M., McClure-Begley, A., Johnson, B. J., Oltmans, S. J. and Tarasick, D.: An assessment of 10-year NOAA aircraft-based tropospheric ozone profiling in Colorado, Atmospheric Environment, 158, 116–127, doi:10.1016/j.atmosenv.2017.03.013, 2017.

Levy, H.: Normal Atmosphere: Large Radical and Formaldehyde Concentrations Predicted, Science, 173(3992), 141–143, doi:10.1126/science.173.3992.141, 1971.

Lin, M., Fiore, A. M., Horowitz, L. W., Langford, A. O., Oltmans, S. J., Tarasick, D. and Rieder, H. E.: Climate variability modulates western US ozone air quality in spring via deep stratospheric intrusions, Nature Communications, 6, 7105, doi:10.1038/ncomms8105, 2015a.

Lin, M., Horowitz, L. W., Cooper, O. R., Tarasick, D. W., Conley, S., Iraci, L. T., Johnson, B. J., Leblanc, T., Petropavlovskikh, I. and Yates, E. L.: Revisiting the evidence of increasing springtime

832 ozone mixing ratios in the free troposphere over western North America, Geophysical Research
833 Letters, 42(20), 8719–8728, doi:10.1002/2015GL065311, 2015b.

834 Lin, M., Horowitz, L. W., Payton, R., Fiore, A. M. and Tonnesen, G.: US surface ozone trends and
835 extremes from 1980 to 2014: quantifying the roles of rising Asian emissions, domestic controls,
836 wildfires, and climate, Atmospheric Chemistry and Physics, 17(4), 2943–2970, doi:10.5194/acp-
837 17-2943-2017, 2017.

838 Liu, G., Tarasick, D. W., Fioletov, V. E., Sioris, C. E. and Rochon, Y. J.: Ozone correlation lengths
839 and measurement uncertainties from analysis of historical ozonesonde data in North America
840 and Europe, Journal of Geophysical Research: Atmospheres, 114(D4),
841 doi:10.1029/2008JD010576, 2009.

842 Liu, G., Liu, J., Tarasick, D. W., Fioletov, V. E., Jin, J. J., Moeini, O., Liu, X., Sioris, C. E. and Osman,
843 M.: A global tropospheric ozone climatology from trajectory-mapped ozone soundings,
844 Atmospheric Chemistry and Physics, 13(21), 10659–10675, doi:10.5194/acp-13-10659-2013,
845 2013.

846 Liu, H., Jacob, D. J., Chan, L. Y., Oltmans, S. J., Bey, I., Yantosca, R. M., Harris, J. M., Duncan, B. N.
847 and Martin, R. V.: Sources of tropospheric ozone along the Asian Pacific Rim: An analysis of
848 ozonesonde observations, Journal of Geophysical Research: Atmospheres, 107(D21), ACH 3-1-
849 ACH 3-19, doi:10.1029/2001JD002005, 2002.

850 Logan, J. A.: Tropospheric ozone: Seasonal behavior, trends, and anthropogenic influence,
851 Journal of Geophysical Research: Atmospheres, 90(D6), 10463–10482,
852 doi:10.1029/JD090iD06p10463, 1985.

853 Logan, J. A. and Kirchhoff, V. W. J. H.: Seasonal variations of tropospheric ozone at Natal, Brazil,
854 Journal of Geophysical Research: Atmospheres, 91(D7), 7875–7881,
855 doi:10.1029/JD091iD07p07875, 1986.

856 Logan, J. A., Staehelin, J., Megretskaia, I. A., Cammas, J. -P., Thouret, Claude, H., Backer, H.,
857 Steinbacher, M., Scheel, H. -E., Stübi, R., Fröhlich, M. and Derwent, R.: Changes in ozone over
858 Europe: Analysis of ozone measurements from sondes, regular aircraft (MOZAIC) and alpine
859 surface sites, Journal of Geophysical Research: Atmospheres, 117(D9),
860 doi:10.1029/2011JD016952, 2012.

861 Marenco, A., Thouret, V., Nédélec, P., Smit, H., Helten, M., Kley, D., Karcher, F., Simon, P., Law,
862 K., Pyle, J., Poschmann, G., Wrede, R. V., Hume, C. and Cook, T.: Measurement of ozone and
863 water vapor by Airbus in-service aircraft: The MOZAIC airborne program, an overview, Journal
864 of Geophysical Research: Atmospheres, 103(D19), 25631–25642, doi:10.1029/98JD00977,
865 1998.

866 Martin, B. D., Fuelberg, H. E., Blake, N. J., Crawford, J. H., Logan, J. A., Blake, D. R. and Sachse, G.
867 W.: Long-range transport of Asian outflow to the equatorial Pacific, Journal of Geophysical
868 Research: Atmospheres, 107(D2), PEM 5-1-PEM 5-18, doi:10.1029/2001JD001418, 2002.

869 Martín, M. V., Honrath, R. E., Owen, R. C., Pfister, G., Fialho, P. and Barata, F.: Significant
870 enhancements of nitrogen oxides, black carbon, and ozone in the North Atlantic lower free
871 troposphere resulting from North American boreal wildfires, Journal of Geophysical Research:
872 Atmospheres, 111(D23), doi:10.1029/2006JD007530, 2006.

873 Mauzerall, D. L., Logan, J. A., Jacob, D. J., Anderson, B. E., Blake, D. R., Bradshaw, J. D., Heikes,
874 B., Sachse, G. W., Singh, H. and Talbot, B.: Photochemistry in biomass burning plumes and
875 implications for tropospheric ozone over the tropical South Atlantic, Journal of Geophysical
876 Research: Atmospheres, 103(D7), 8401–8423, doi:10.1029/97JD02612, 1998.

877 Monks, P. S.: A review of the observations and origins of the spring ozone maximum,
878 Atmospheric Environment, 34(21), 3545–3561, doi:10.1016/S1352-2310(00)00129-1, 2000.

879 Monks, P. S., Carpenter, L. J., Penkett, S. A., Ayers, G. P., Gillett, R. W., Galbally, I. E. and (Mick)
880 Meyer, C. P.: Fundamental ozone photochemistry in the remote marine boundary layer: the
881 soapex experiment, measurement and theory, Atmospheric Environment, 32(21), 3647–3664,
882 doi:10.1016/S1352-2310(98)00084-3, 1998.

883 Monks, P. S., Salisbury, G., Holland, G., Penkett, S. A. and Ayers, G. P.: A seasonal comparison of
884 ozone photochemistry in the remote marine boundary layer, Atmospheric Environment, 34(16),
885 2547–2561, doi:10.1016/S1352-2310(99)00504-X, 2000.

886 Monks, P. S., Granier, C., Fuzzi, S., Stohl, A., Williams, M. L., Akimoto, H., Amann, M., Baklanov,
887 A., Baltensperger, U., Bey, I., Blake, N., Blake, R. S., Carslaw, K., Cooper, O. R., Dentener, F.,
888 Fowler, D., Fragkou, E., Frost, G. J., Generoso, S., Ginoux, P., Grewe, V., Guenther, A., Hansson,
889 H. C., Henne, S., Hjorth, J., Hofzumahaus, A., Huntrieser, H., Isaksen, I. S. A., Jenkin, M. E.,
890 Kaiser, J., Kanakidou, M., Klimont, Z., Kulmala, M., Laj, P., Lawrence, M. G., Lee, J. D., Liousse, C.,
891 Maione, M., McFiggans, G., Metzger, A., Mieville, A., Moussiopoulos, N., Orlando, J. J., O'Dowd,
892 C. D., Palmer, P. I., Parrish, D. D., Petzold, A., Platt, U., Pöschl, U., Prévôt, A. S. H., Reeves, C. E.,
893 Reimann, S., Rudich, Y., Sellegri, K., Steinbrecher, R., Simpson, D., ten Brink, H., Theloke, J., van
894 der Werf, G. R., Vautard, R., Vestreng, V., Vlachokostas, Ch. and von Glasow, R.: Atmospheric
895 composition change – global and regional air quality, Atmospheric Environment, 43(33), 5268–
896 5350, doi:10.1016/j.atmosenv.2009.08.021, 2009.

897 Moxim, W. J. and Levy, H.: A model analysis of the tropical South Atlantic Ocean tropospheric
898 ozone maximum: The interaction of transport and chemistry, Journal of Geophysical Research:
899 Atmospheres, 105(D13), 17393–17415, doi:10.1029/2000JD900175, 2000.

900 Nath, D., Chen, W., Graf, H.-F., Lan, X., Gong, H., Nath, R., Hu, K. and Wang, L.: Subtropical
901 Potential Vorticity Intrusion Drives Increasing Tropospheric Ozone over the Tropical Central
902 Pacific, Scientific Reports, 6, 21370, doi:10.1038/srep21370, 2016.

Nédélec, P., Cammas, J.-P., Thouret, V., Athier, G., Cousin, J.-M., Legrand, C., Abonnel, C., Lecoeur, F., Cayez, G. and Marizy, C.: An improved infrared carbon monoxide analyser for routine measurements aboard commercial Airbus aircraft: technical validation and first scientific results of the MOZAIC III programme, Atmospheric Chemistry and Physics, 3(5), 1551–1564, doi:https://doi.org/10.5194/acp-3-1551-2003, 2003.

Nédélec, P., Blot, R., Boulanger, D., Athier, G., Cousin, J.-M., Gautron, B., Petzold, A., Volz-Thomas, A. and Thouret, V.: Instrumentation on commercial aircraft for monitoring the atmospheric composition on a global scale: the IAGOS system, technical overview of ozone and carbon monoxide measurements, Tellus B: Chemical and Physical Meteorology, 68(s1), 27791, doi:10.3402/tellusb.v67.27791, 2015.

Neuman, J. A., Trainer, M., Aikin, K. C., Angevine, W. M., Brioude, J., Brown, S. S., de Gouw, J. A., Dube, W. P., Flynn, J. H., Graus, M., Holloway, J. S., Lefer, B. L., Nedelec, P., Nowak, J. B., Parrish, D. D., Pollack, I. B., Roberts, J. M., Ryerson, T. B., Smit, H., Thouret, V. and Wagner, N. L.: Observations of ozone transport from the free troposphere to the Los Angeles basin, Journal of Geophysical Research: Atmospheres, 117(D21), n/a-n/a, doi:10.1029/2011JD016919, 2012.

Newell, R. E. and Evans, M. J.: Seasonal changes in pollutant transport to the North Pacific: The relative importance of Asian and European sources, Geophysical Research Letters, 27(16), 2509–2512, doi:10.1029/2000GL011501, 2000.

Newton, R., Vaughan, G., Hintsa, E., Filus, M. T., Pan, L. L., Honomichl, S., Atlas, E., Andrews, S. J. and Carpenter, L. J.: Observations of ozone-poor air in the Tropical Tropopause Layer, Atmospheric Chemistry and Physics Discussions, 1–23, doi:10.5194/acp-2017-970, 2017.

Oltmans, S. J., Johnson, B. J., Harris, J. M., Vömel, H., Thompson, A. M., Koshy, K., Simon, P., Bendura, R. J., Logan, J. A., Hasebe, F., Shiotani, M., Kirchhoff, V. W. J. H., Maata, M., Sami, G., Samad, A., Tabuadravu, J., Enriquez, H., Agama, M., Cornejo, J. and Paredes, F.: Ozone in the Pacific tropical troposphere from ozonesonde observations, Journal of Geophysical Research: Atmospheres, 106(D23), 32503–32525, doi:10.1029/2000JD900834, 2001.

Oltmans, S. J., Lefohn, A. S., Shadwick, D., Harris, J. M., Scheel, H. E., Galbally, I., Tarasick, D. W., Johnson, B. J., Brunke, E.-G., Claude, H., Zeng, G., Nichol, S., Schmidlin, F., Davies, J., Cuevas, E., Redondas, A., Naoe, H., Nakano, T. and Kawasato, T.: Recent tropospheric ozone changes – A pattern dominated by slow or no growth, Atmospheric Environment, 67, 331–351, doi:10.1016/j.atmosenv.2012.10.057, 2013.

Owen, R. C., Cooper, O. R., Stohl, A. and Honrath, R. E.: An analysis of the mechanisms of North American pollutant transport to the central North Atlantic lower free troposphere, Journal of Geophysical Research: Atmospheres, 111(D23), doi:10.1029/2006JD007062, 2006.

Pan, L. L., Honomichl, S. B., Randel, W. J., Apel, E. C., Atlas, E. L., Beaton, S. P., Bresch, J. F., Hornbrook, R., Kinnison, D. E., Lamarque, J.-F., Saiz-Lopez, A., Salawitch, R. J. and Weinheimer, A. J.: Bimodal distribution of free tropospheric ozone over the tropical western Pacific revealed

940 by airborne observations, Geophysical Research Letters, 42(18), 7844–7851,
941 doi:10.1002/2015GL065562, 2015.

942 Parrish, D. D., Galbally, I. E., Lamarque, J. -F., Naik, V., Horowitz, Shindell, D. T., Oltmans, S. J.,
943 Derwent, R., Tanimoto, H., Labuschagne, C. and Cupeiro, M.: Seasonal cycles of O3 in the
944 marine boundary layer: Observation and model simulation comparisons, Journal of Geophysical
945 Research: Atmospheres, 121(1), 538–557, doi:10.1002/2015JD024101, 2016.

946 Parrish, D. D., Derwent, R. G., Steinbrecht, W., Stübi, R., Malderen, R. V., Steinbacher, M., Trickl,
947 T., Ries, L. and Xu, X.: Zonal Similarity of Long-term Changes and Seasonal Cycles of Baseline
948 Ozone at Northern Mid-latitudes, Journal of Geophysical Research: Atmospheres, n/a(n/a),
949 e2019JD031908, doi:10.1029/2019JD031908, 2020.

950 Perkins, S. E., Pitman, A. J., Holbrook, N. J. and McAneney, J.: Evaluation of the AR4 Climate
951 Models' Simulated Daily Maximum Temperature, Minimum Temperature, and Precipitation
952 over Australia Using Probability Density Functions, J. Climate, 20(17), 4356–4376,
953 doi:10.1175/JCLI4253.1, 2007.

954 Petetin, H., Thouret, V., Fontaine, A., Sauvage, B., Athier, G., Blot, R., Boulanger, D., Cousin, J.-
955 M. and Nédélec, P.: Characterising tropospheric O3 and CO around Frankfurt over the period
956 1994–2012 based on MOZAIC–IAGOS aircraft measurements, Atmos. Chem. Phys., 16(23),
957 15147–15163, doi:10.5194/acp-16-15147-2016, 2016.

958 Petzold, A., Thouret, V., Gerbig, C., Zahn, A., Brenninkmeijer, C. A. M., Gallagher, M., Hermann,
959 M., Pontaud, M., Ziereis, H., Boulanger, D., Marshall, J., Nédélec, P., Smit, H. G. J., Friess, U.,
960 Flaud, J.-M., Wahner, A., Cammas, J.-P., Volz-Thomas, A. and TEAM, I.: Global-scale atmosphere
961 monitoring by in-service aircraft – current achievements and future prospects of the European
962 Research Infrastructure IAGOS, Tellus B: Chemical and Physical Meteorology, 67(1), 28452,
963 doi:10.3402/tellusb.v67.28452, 2015.

964 Pickering, K. E., Thompson, A. M., Wang, Y., Tao, W.-K., McNamara, D. P., Kirchhoff, V. W. J. H.,
965 Heikes, B. G., Sachse, G. W., Bradshaw, J. D., Gregory, G. L. and Blake, D. R.: Convective
966 transport of biomass burning emissions over Brazil during TRACE A, Journal of Geophysical
967 Research: Atmospheres, 101(D19), 23993–24012, doi:10.1029/96JD00346, 1996.

968 Prather, M. J., Zhu, X., Flynn, C. M., Strode, S. A., Rodriguez, J. M., Steenrod, S. D., Liu, J.,
969 Lamarque, J.-F., Fiore, A. M., Horowitz, L. W., Mao, J., Murray, L. T., Shindell, D. T. and Wofsy, S.
970 C.: Global atmospheric chemistry – which air matters, Atmospheric Chemistry and Physics,
971 17(14), 9081–9102, doi:https://doi.org/10.5194/acp-17-9081-2017, 2017.

972 Proffitt, M. H. and McLaughlin, R. J.: Fast-response dual-beam UV-absorption ozone
973 photometer suitable for use on stratospheric balloons, Review of Scientific Instruments, 54(12),
974 1719–1728, doi:10.1063/1.1137316, 1983.

975 Ridley, B. A., Grahek, F. E. and Walega, J. G.: A Small High-Sensitivity, Medium-Response Ozone
976 Detector Suitable for Measurements from Light Aircraft, J. Atmos. Oceanic Technol., 9(2), 142–
977 148, doi:10.1175/1520-0426(1992)009<0142:ASHSMR>2.0.CO;2, 1992.

978 Santoni, G. W., Daube, B. C., Kort, E. A., Jiménez, R., Park, S., Pittman, J. V., Gottlieb, E., Xiang,
979 B., Zahniser, M. S., Nelson, D. D., McManus, J. B., Peischl, J., Ryerson, T. B., Holloway, J. S.,
980 Andrews, A. E., Sweeney, C., Hall, B., Hintsa, E. J., Moore, F. L., Elkins, J. W., Hurst, D. F.,
981 Stephens, B. B., Bent, J. and Wofsy, S. C.: Evaluation of the airborne quantum cascade laser
982 spectrometer (QCLS) measurements of the carbon and greenhouse gas suite – CO_2, CH_4,
983 N_2O, and CO – during the CalNex and HIPPO campaigns, Atmospheric Measurement
984 Techniques, 7(6), 1509–1526, doi:https://doi.org/10.5194/amt-7-1509-2014, 2014.

985 Sauvage, B., Thouret, V., Thompson, A. M., Witte, J. C., Cammas, J.-P., Nédélec, P. and Athier,
986 G.: Enhanced view of the "tropical Atlantic ozone paradox" and "zonal wave one" from the in
987 situ MOZAIC and SHADOZ data, Journal of Geophysical Research: Atmospheres, 111(D1),
988 doi:10.1029/2005JD006241, 2006.

989 Schultz, M. G., Jacob, D. J., Wang, Y., Logan, J. A., Atlas, E. L., Blake, D. R., Blake, N. J., Bradshaw,
990 J. D., Browell, E. V., Fenn, M. A., Flocke, F., Gregory, G. L., Heikes, B. G., Sachse, G. W.,
991 Sandholm, S. T., Shetter, R. E., Singh, H. B. and Talbot, R. W.: On the origin of tropospheric
992 ozone and NO_x over the tropical South Pacific, Journal of Geophysical Research: Atmospheres,
993 104(D5), 5829–5843, doi:10.1029/98JD02309, 1999.

994 Shen, Z., Liu, J., Horowitz, L. W., Henze, D. K., Fan, S., H., L. I., Mauzerall, D. L., Lin, J.-T. and Tao,
995 S.: Analysis of transpacific transport of black carbon during HIPPO-3: implications for black
996 carbon aging, Atmospheric Chemistry and Physics, 14(12), 6315–6327, doi:10.5194/acp-14-
997 6315-2014, 2014.

998 Shindell, D., Kuylenstierna, J. C. I., Vignati, E., Dingenen, R. van, Amann, M., Klimont, Z.,
999 Anenberg, S. C., Muller, N., Janssens-Maenhout, G., Raes, F., Schwartz, J., Faluvegi, G., Pozzoli,
1000 L., Kupiainen, K., Höglund-Isaksson, L., Emberson, L., Streets, D., Ramanathan, V., Hicks, K.,
1001 Oanh, N. T. K., Milly, G., Williams, M., Demkine, V. and Fowler, D.: Simultaneously Mitigating
1002 Near-Term Climate Change and Improving Human Health and Food Security, Science,
1003 335(6065), 183–189, doi:10.1126/science.1210026, 2012.

1004 Singh, H. B., Herlth, D., Kolyer, R., Chatfield, R., Viezee, W., Salas, L. J., Chen, Y., Bradshaw, J. D.,
1005 Sandholm, S. T., Talbot, R., Gregory, G. L., Anderson, B., Sachse, G. W., Browell, E., Bachmeier,
1006 A. S., Blake, D. R., Heikes, B., Jacob, D. and Fuelberg, H. E.: Impact of biomass burning emissions
1007 on the composition of the South Atlantic troposphere: Reactive nitrogen and ozone, Journal of
1008 Geophysical Research: Atmospheres, 101(D19), 24203–24219, doi:10.1029/96JD01018, 1996a.

1009 Singh, H. B., Gregory, G. L., Anderson, B., Browell, E., Sachse, G. W., Davis, D. D., Crawford, J.,
1010 Bradshaw, J. D., Talbot, R., Blake, D. R., Thornton, D., Newell, R. and Merrill, J.: Low ozone in the
1011 marine boundary layer of the tropical Pacific Ocean: Photochemical loss, chlorine atoms, and

1012 entrainment, Journal of Geophysical Research: Atmospheres, 101(D1), 1907–1917,
1013 doi:10.1029/95JD01028, 1996b.

1014 Singh, H. B., Herlth, D., Kolyer, R., Salas, L., Bradshaw, J. D., Sandholm, S. T., Davis, D. D.,
1015 Crawford, J., Kondo, Y., Koike, M., Talbot, R., Gregory, G. L., Sachse, G. W., Browell, E., Blake, D.
1016 R., Rowland, F. S., Newell, R., Merrill, J., Heikes, B., Liu, S. C., Crutzen, P. J. and Kanakidou, M.:
1017 Reactive nitrogen and ozone over the western Pacific: Distribution, partitioning, and sources, J.
1018 Geophys. Res., 101(D1), 1793–1808, doi:10.1029/95JD01029, 1996c.

1019 Solomon, S., Thompson, D. W. J., Portmann, R. W., Oltmans, S. J. and Thompson, A. M.: On the
1020 distribution and variability of ozone in the tropical upper troposphere: Implications for tropical
1021 deep convection and chemical-dynamical coupling, Geophysical Research Letters, 32(23),
1022 doi:10.1029/2005GL024323, 2005.

1023 Stauffer, R. M., Thompson, A. M. and Witte, J. C.: Characterizing Global Ozonesonde Profile
1024 Variability From Surface to the UT/LS With a Clustering Technique and MERRA-2 Reanalysis,
1025 Journal of Geophysical Research: Atmospheres, 123(11), 6213–6229,
1026 doi:10.1029/2018JD028465, 2018.

1027 Stedman, D. H., Daby, E. E., Stuhl, F. and Niki, H.: Analysis of Ozone and Nitric Oxide by a
1028 Chemiluminescent Method in Laboratory and Atmospheric Studies of Photochemical Smog,
1029 Journal of the Air Pollution Control Association, 22(4), 260–263,
1030 doi:10.1080/00022470.1972.10469635, 1972.

1031 Tarasick, D. W. and Bottenheim, J. W.: Surface ozone depletion episodes in the Arctic and
1032 Antarctic from historical ozonesonde records, Atmospheric Chemistry and Physics, 2(3), 197–
1033 205, doi:https://doi.org/10.5194/acp-2-197-2002, 2002.

1034 Tarasick, D. W., Jin, J. J., Fioletov, V. E., Liu, G., Thompson, A. M., Oltmans, S. J., Liu, J., Sioris, C.
1035 E., Liu, X., Cooper, O. R., Dann, T. and Thouret, V.: High-resolution tropospheric ozone fields for
1036 INTEX and ARCTAS from IONS ozonesondes, Journal of Geophysical Research: Atmospheres,
1037 115(D20), doi:10.1029/2009JD012918, 2010.

1038 Tarasick, D. W., Carey-Smith, T. K., Hocking, W. K., Moeini, O., He, H., Liu, J., Osman, M. K.,
1039 Thompson, A. M., Johnson, B. J., Oltmans, S. J. and Merrill, J. T.: Quantifying stratosphere-
1040 troposphere transport of ozone using balloon-borne ozonesondes, radar windprofilers and
1041 trajectory models, Atmospheric Environment, 198, 496–509,
1042 doi:10.1016/j.atmosenv.2018.10.040, 2019a.

1043 Tarasick, D. W., Galbally, I. E., Cooper, O. R., Schultz, M. G., Ancellet, G., Leblanc, T., Wallington,
1044 T. J., Ziemke, J., Liu, X., Steinbacher, M., Staehelin, J., Vigouroux, C., Hannigan, J. W., García, O.,
1045 Foret, G., Zanis, P., Weatherhead, E., Petropavlovskikh, I., Worden, H., Osman, M., Liu, J.,
1046 Chang, K.-L., Gaudel, A., Lin, M., Granados-Muñoz, M., Thompson, A. M., Oltmans, S. J., Cuesta,
1047 J., Dufour, G., Thouret, V., Hassler, B., Trickl, T. and Neu, J. L.: Tropospheric Ozone Assessment

1048 Report: Tropospheric ozone from 1877 to 2016, observed levels, trends and uncertainties, Elem
1049 Sci Anth, 7(1), 39, doi:10.1525/elementa.376, 2019b.

1050 Thompson, A. M., Johnson, J. E., Torres, A. L., Bates, T. S., Kelly, K. C., Atlas, E., Greenberg, J. P.,
1051 Donahue, N. M., Yvon, S. A., Saltzman, E. S., Heikes, B. G., Mosher, B. W., Shashkov, A. A. and
1052 Yegorov, V. I.: Ozone observations and a model of marine boundary layer photochemistry
1053 during SAGA 3, Journal of Geophysical Research: Atmospheres, 98(D9), 16955–16968,
1054 doi:10.1029/93JD00258, 1993.

1055 Thompson, A. M., Pickering, K. E., McNamara, D. P., Schoeberl, M. R., Hudson, R. D., Kim, J. H.,
1056 Browell, E. V., Kirchhoff, V. W. J. H. and Nganga, D.: Where did tropospheric ozone over
1057 southern Africa and the tropical Atlantic come from in October 1992? Insights from TOMS, GTE
1058 TRACE A, and SAFARI 1992, Journal of Geophysical Research: Atmospheres, 101(D19), 24251–
1059 24278, doi:10.1029/96JD01463, 1996.

1060 Thompson, A. M., Doddridge, B. G., Witte, J. C., Hudson, R. D., Luke, W. T., Johnson, J. E.,
1061 Johnson, B. J., Oltmans, S. J. and Weller, R.: A tropical Atlantic Paradox: Shipboard and satellite
1062 views of a tropospheric ozone maximum and wave-one in January–February 1999, Geophysical
1063 Research Letters, 27(20), 3317–3320, doi:10.1029/1999GL011273, 2000.

1064 Thompson, A. M., Miller, S. K., Tilmes, S., Kollonige, D. W., Witte, J. C., Oltmans, S. J., Johnson,
1065 B. J., Fujiwara, M., Schmidlin, F. J., Coetzee, G. J. R., Komala, N., Maata, M., Mohamad, M. B.,
1066 Nguyo, J., Mutai, C., Ogino, S. Y., Silva, F. R. D., Leme, N. M. P., Posny, F., Scheele, R., Selkirk, H.
1067 B., Shiotani, M., Stbi, R., Levrat, G., Calpini, B., Thouret, V., Tsuruta, H., Canossa, J. V., Vmel, H.,
1068 Yonemura, S., Diaz, J. A., Thanh, N. T. T. and Ha, H. T. T.: Southern Hemisphere Additional
1069 Ozonesondes (SHADOZ) ozone climatology (2005-2009): Tropospheric and tropical tropopause
1070 layer (TTL) profiles with comparisons to OMI-based ozone products, Journal of Geophysical
1071 Research Atmospheres, 117(23), D23301, doi:10.1029/2011JD016911, 2012.

1072 Thompson, A. M., Witte, J. C., Sterling, C., Jordan, A., Johnson, B. J., Oltmans, S. J., Fujiwara, M.,
1073 Vömel, H., Allaart, M., Piters, A., Coetzee, G. J. R., Posny, F., Corrales, E., Diaz, J. A., Félix, C.,
1074 Komala, N., Lai, N., Ahn Nguyen, H. T., Maata, M., Mani, F., Zainal, Z., Ogino, S., Paredes, F.,
1075 Penha, T. L. B., da Silva, F. R., Sallons-Mitro, S., Selkirk, H. B., Schmidlin, F. J., Stübi, R. and
1076 Thiongo, K.: First Reprocessing of Southern Hemisphere Additional Ozonesondes (SHADOZ)
1077 Ozone Profiles (1998-2016): 2. Comparisons With Satellites and Ground-Based Instruments:
1078 SHADOZ Data Evaluation, Journal of Geophysical Research: Atmospheres,
1079 doi:10.1002/2017JD027406, 2017.

1080 Thompson, A. M., Smit, H. G. J., Witte, J. C., Stauffer, R. M., Johnson, B. J., Morris, G., von der
1081 Gathen, P., Van Malderen, R., Davies, J., Piters, A., Allaart, M., Posny, F., Kivi, R., Cullis, P., Hoang
1082 Anh, N. T., Corrales, E., Machinini, T., da Silva, F. R., Paiman, G., Thiong'o, K., Zainal, Z., Brothers,
1083 G. B., Wolff, K. R., Nakano, T., Stübi, R., Romanens, G., Coetzee, G. J. R., Diaz, J. A., Mitro, S.,
1084 Mohamad, M. and Ogino, S.-Y.: Ozonesonde Quality Assurance: The JOSIE–SHADOZ (2017)
1085 Experience, Bull. Amer. Meteor. Soc., 100(1), 155–171, doi:10.1175/BAMS-D-17-0311.1, 2019.

1086 Thompson, C. R., Ryerson, T. B., Peischl, J., Barletta, B., Blake, D. R., Butler, A. H., Crounse, J. D.,
1087 Evans, M. J., Fisher, J. A., Huey, L. G., Kim, M. J., Laubach, A., Moore, F. L., Ray, E. A., Murray, L.
1088 T., Sherwen, T., Strode, S. A., Wennberg, P. O. and Yu, P.: Global-scale Airborne Observations of
1089 Tropospheric Reactive Nitrogen Species from the NASA Atmospheric Tomography Mission, AGU
1090 Fall Meeting Abstracts, 14 [online] Available from:
1091 http://adsabs.harvard.edu/abs/2017AGUFM.A14D..02T (Accessed 16 March 2020b), 2017.

1092 Thouret, V., Marenco, A., Logan, J. A., Nédélec, P. and Grouhel, C.: Comparisons of ozone
1093 measurements from the MOZAIC airborne program and the ozone sounding network at eight
1094 locations, Journal of Geophysical Research: Atmospheres, 103(D19), 25695–25720,
1095 doi:10.1029/98JD02243, 1998.

1096 Tilmes, S., Lamarque, J.-F., Emmons, L. K., Conley, A., Schultz, M. G., Saunois, M., Thouret, V.,
1097 Thompson, A. M., Oltmans, S. J., Johnson, B. and Tarasick, D.: Technical Note: Ozonesonde
1098 climatology between 1995 and 2011: description, evaluation and applications, Atmospheric
1099 Chemistry and Physics, 12(16), 7475–7497, doi:https://doi.org/10.5194/acp-12-7475-2012,
1100 2012.

1101 Trickl, T., Cooper, O. R., Eisele, H., James, P., Mücke, R. and Stohl, A.: Intercontinental transport
1102 and its influence on the ozone concentrations over central Europe: Three case studies, Journal
1103 of Geophysical Research: Atmospheres, 108(D12), doi:10.1029/2002JD002735, 2003.

1104 Wespes, C., Hurtmans D., Clerbaux C. and Coheur P.-F.: O3 variability in the troposphere as
1105 observed by IASI over 2008–2016: Contribution of atmospheric chemistry and dynamics,
1106 Journal of Geophysical Research: Atmospheres, 122(4), 2429–2451,
1107 doi:10.1002/2016JD025875, 2017.

1108 Williams, J. E., Scheele, M. P., van Velthoven, P. F. J., Thouret, V., Saunois, M., Reeves, C. E. and
1109 Cammas, J.-P.: The influence of biomass burning and transport on tropospheric composition
1110 over the tropical Atlantic Ocean and Equatorial Africa during the West African monsoon in
1111 2006, Atmospheric Chemistry and Physics, 10(20), 9797–9817, doi:10.5194/acp-10-9797-2010,
1112 2010.

1113 Witte, J. C., Thompson, A. M., Smit, H. G. J., Vömel, H., Posny, F. and Stübi, R.: First
1114 Reprocessing of Southern Hemisphere ADditional OZonesondes Profile Records: 3. Uncertainty
1115 in Ozone Profile and Total Column, Journal of Geophysical Research: Atmospheres, 123(6),
1116 3243–3268, doi:10.1002/2017JD027791, 2018.

1117 Wofsy, S. C.: HIAPER Pole-to-Pole Observations (HIPPO): fine-grained, global-scale
1118 measurements of climatically important atmospheric gases and aerosols, Philosophical
1119 Transactions of the Royal Society A: Mathematical, Physical and Engineering Sciences,
1120 369(1943), 2073–2086, doi:10.1098/rsta.2010.0313, 2011.

1121 Young, P. J., Archibald, A. T., Bowman, K. W., Lamarque, J.-F., Naik, V., Stevenson, D. S., Tilmes,
1122 S., Voulgarakis, A., Wild, O., Bergmann, D., Cameron-Smith, P., Cionni, I., Collins, W. J., Dalsøren,

S. B., Doherty, R. M., Eyring, V., Faluvegi, G., Horowitz, L. W., Josse, B., Lee, Y. H., MacKenzie, I. A., Nagashima, T., Plummer, D. A., Righi, M., Rumbold, S. T., Skeie, R. B., Shindell, D. T., Strode, S. A., Sudo, K., Szopa, S. and Zeng, G.: Pre-industrial to end 21st century projections of tropospheric ozone from the Atmospheric Chemistry and Climate Model Intercomparison Project (ACCMIP), Atmos. Chem. Phys., 13(4), 2063–2090, doi:10.5194/acp-13-2063-2013, 2013.

Young, P. J., Naik, V., Fiore, A. M., Gaudel, A., Guo, J., Lin, M. Y., Neu, J. L., Parrish, D. D., Rieder, H. E., Schnell, J. L., Tilmes, S., Wild, O., Zhang, L., Ziemke, J. R., Brandt, J., Delcloo, A., Doherty, R. M., Geels, C., Hegglin, M. I., Hu, L., Im, U., Kumar, R., Luhar, A., Murray, L., Plummer, D., Rodriguez, J., Saiz-Lopez, A., Schultz, M. G., Woodhouse, M. T. and Zeng, G.: Tropospheric Ozone Assessment Report: Assessment of global-scale model performance for global and regional ozone distributions, variability, and trends, Elem Sci Anth, 6(1), doi:10.1525/elementa.265, 2018.

Zbinden, R. M., Thouret, V., Ricaud, P., Carminati, F., Cammas, J.-P. and Nédélec, P.: Climatology of pure tropospheric profiles and column contents of ozone and carbon monoxide using MOZAIC in the mid-northern latitudes (24° N to 50° N) from 1994 to 2009, Atmospheric Chemistry and Physics, 13(24), 12363–12388, doi:https://doi.org/10.5194/acp-13-12363-2013, 2013.

Zhang, B., Owen, R. C., Perlinger, J. A., Helmig, D., Martín, M. V., Kramer, L., Mazzoleni, L. R. and Mazzoleni, C.: Ten-year chemical signatures associated with long-range transport observed in the free troposphere over the central North Atlantic, Elem Sci Anth, 5(0), doi:10.1525/elementa.194, 2017.

Zhang, L., Jacob, D. J., Boersma, K. F., Jaffe, D. A., Olson, J. R., Bowman, K. W., Worden, J. R., Thompson, A. M., Avery, M. A., Cohen, R. C., Dibb, J. E., Flock, F. M., Fuelberg, H. E., Huey, L. G., McMillan, W. W., Singh, H. B. and Weinheimer, A. J.: Transpacific transport of ozone pollution and the effect of recent Asian emission increases on air quality in North America: an integrated analysis using satellite, aircraft, ozonesonde, and surface observations, Atmospheric Chemistry and Physics, 8(20), 6117–6136, doi:https://doi.org/10.5194/acp-8-6117-2008, 2008.

Ziemke, J. R., Chandra S. and Bhartia P. K.: A 25-year data record of atmospheric ozone in the Pacific from Total Ozone Mapping Spectrometer (TOMS) cloud slicing: Implications for ozone trends in the stratosphere and troposphere, Journal of Geophysical Research: Atmospheres, 110(D15), doi:10.1029/2004JD005687, 2005.

Ziemke, J. R., Chandra S., Duncan B. N., Froidevaux L., Bhartia P. K., Levelt P. F. and Waters J. W.: Tropospheric ozone determined from Aura OMI and MLS: Evaluation of measurements and comparison with the Global Modeling Initiative's Chemical Transport Model, Journal of Geophysical Research: Atmospheres, 111(D19), doi:10.1029/2006JD007089, 2006.

Ziemke, J. R., Strode, S. A., Douglass, A. R., Joiner, J., Vasilkov, A., Oman, L. D., Liu, J., Strahan, S. E., Bhartia, P. K. and Haffner, D. P.: A cloud-ozone data product from Aura OMI and MLS

satellite measurements, Atmos. Meas. Tech., 10(11), 4067–4078, doi:10.5194/amt-10-4067-2017, 2017.

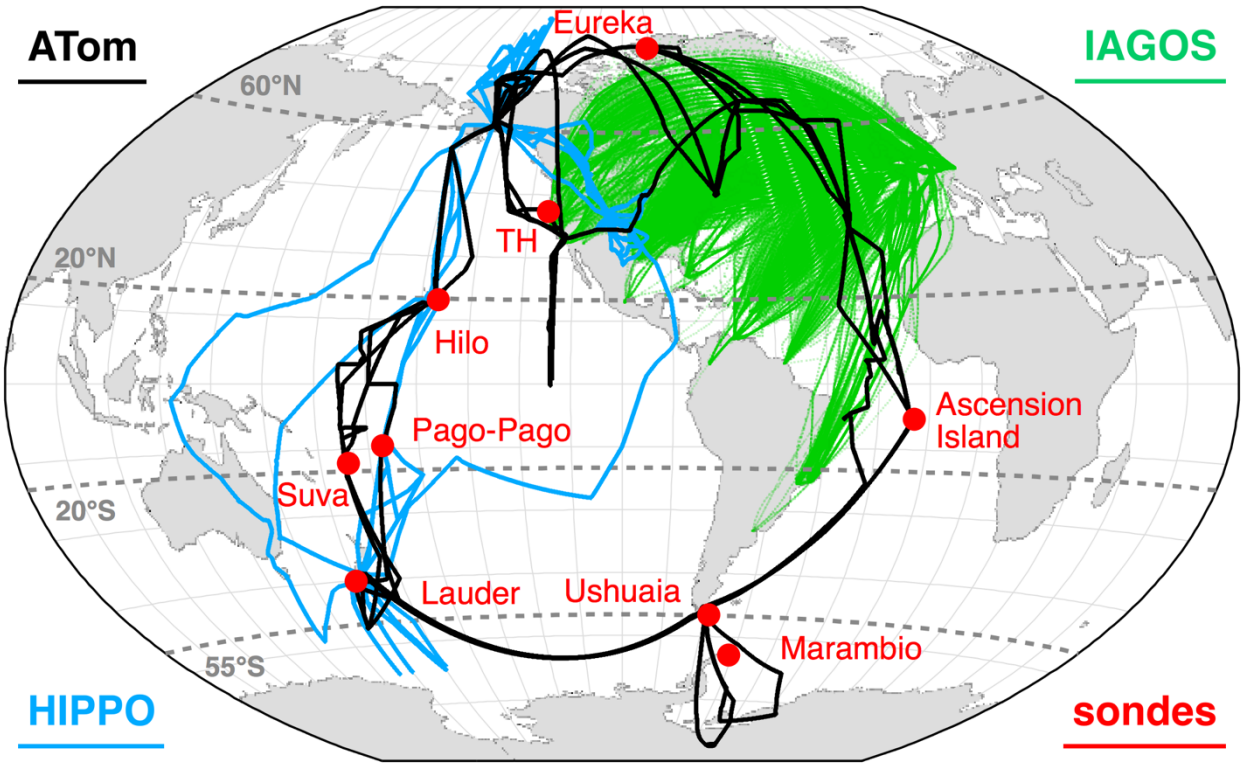

Figure 1 The location and flight tracks of all O_3 monitoring platforms used in this work are illustrated with different markers and colors. The ATom flight track is in black, the HIPPO flight track is in blue, IAGOS flight paths are in green, and the ozonesonde launching sites are indicated by the red markers. The dotted grey lines define the latitudinal bands over which individual ATom and HIPPO profiles were averaged to derive a regional O_3 distribution: the tropics (20° S – 20° N), the midlatitudes (55° S – 20° S; 20° N – 60° N), and the high-latitudes (90° S – 55° S; 60° N – 90° N). Only data from remote oceanic flight segments of ATom and HIPPO missions were used in this work.

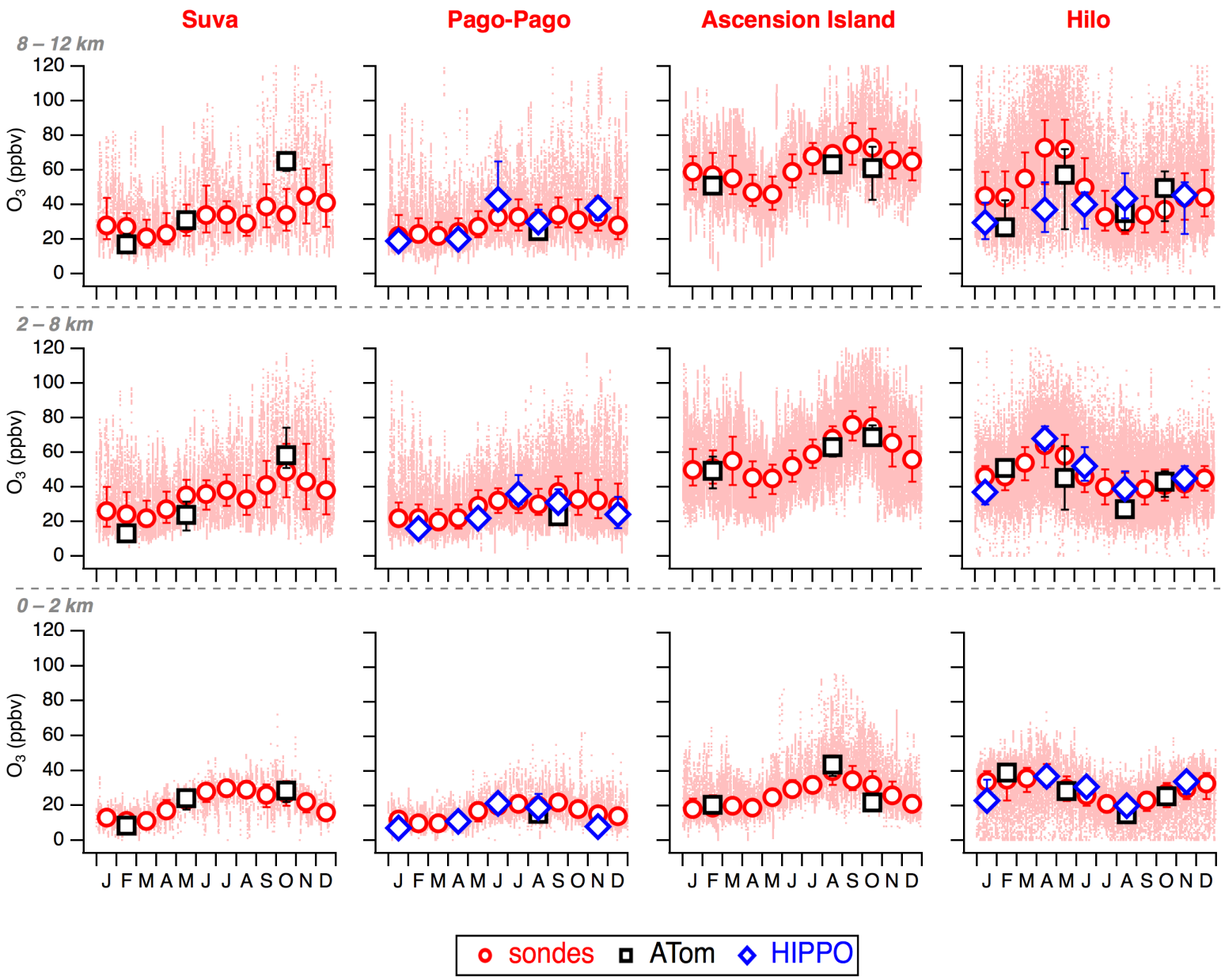
Suva
Pago-Pago
Ascension Island
Hilo
8 – 12 km
2 – 8 km
0 – 2 km
O3 (ppbv)
0
20
40
60
80
100
120
J F M A M J J A S O N D
sondes
ATom
HIPPO

Figure 2 Comparison of ATom (black squares) and HIPPO (blue diamonds) monthly median O_3 with ozonesonde (red circles) records from the four tropical sites. Markers indicate the median and the bars indicate the 25th and 75th percentiles. The three rows, from bottom to top, correspond to the boundary layer (0–2 km), the free troposphere (2–8 km), and the UTLS (8–12 km). The pink dots show every O_3 data point measured by ozonesondes for the timeframes indicated in Table S2.

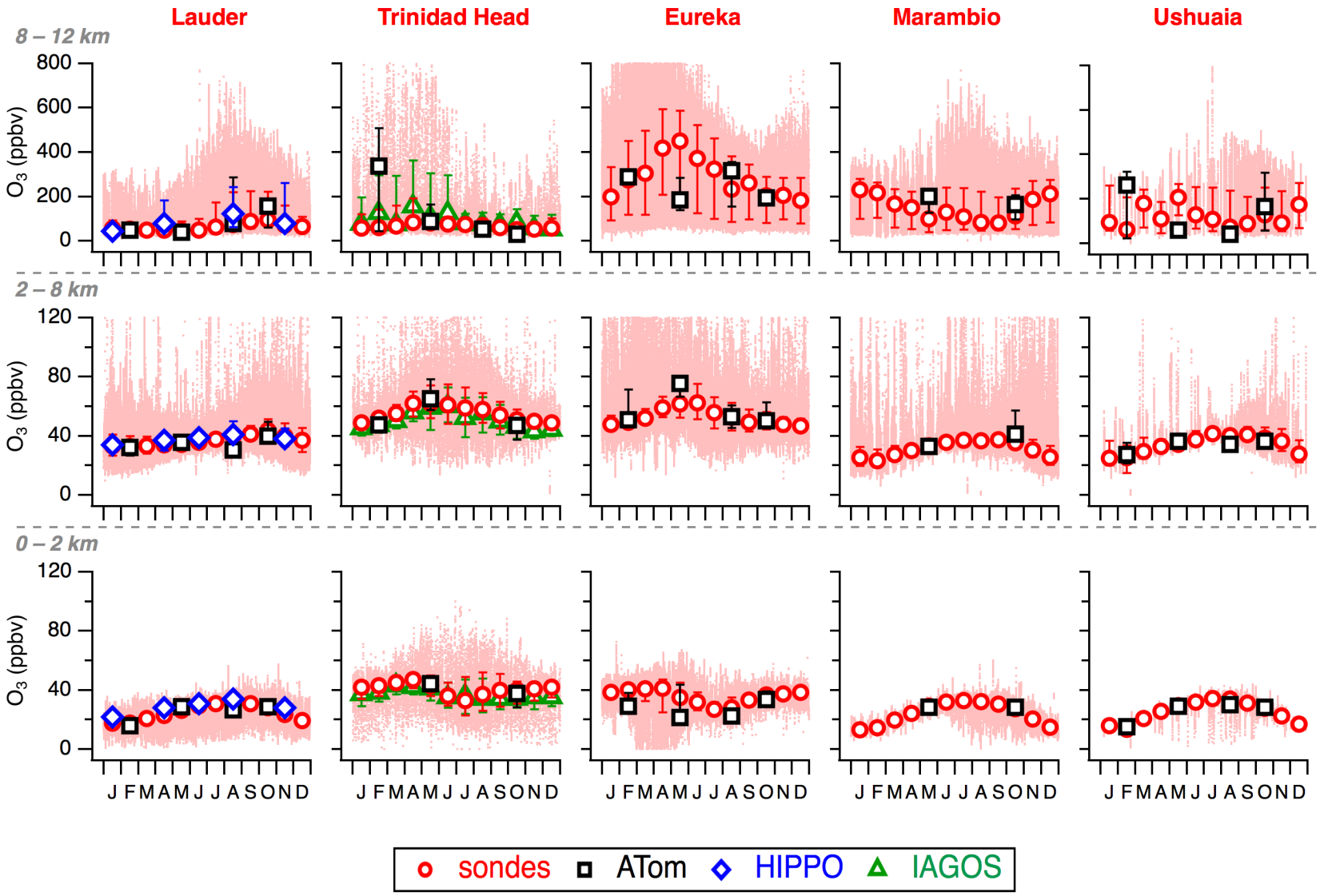
Lauder
Trinidad Head
Eureka
Marambio
Ushuaia
8 – 12 km
2 – 8 km
0 – 2 km
O3 (ppbv)
800
600
400
200
0
120
80
40
0
J F M A M J J A S O N D
sondes
ATom
HIPPO
IAGOS

Figure 3 Same as in Figure 2 but for ozonesonde launching sites located in the middle- and high-latitudes. O_3 data obtained from the IAGOS program (green triangles) during descents into San Francisco Bay-area airports were also added to the Trinidad Head site for comparison.

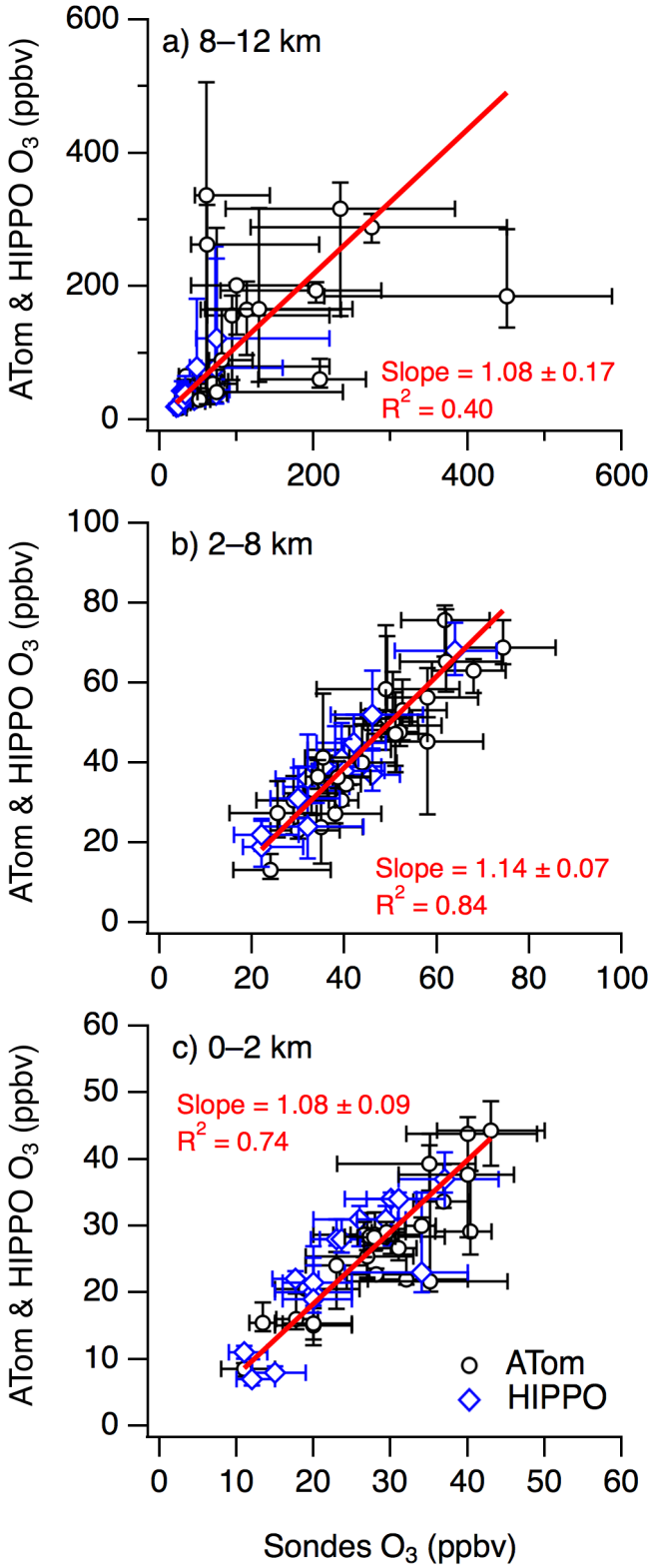

Figure 4 ATom (black circles) and HIPPO (blue diamonds) combined monthly median O_3 vs. monthly median O_3 from ozonesondes at the nine sites considered in this study. The three panels

indicate the correlations for a) the UTLS (8–12 km), b) the free troposphere (2–8 km), and c) the boundary layer (0–2 km). The orthogonal regression fits are two-sided but not weighted.

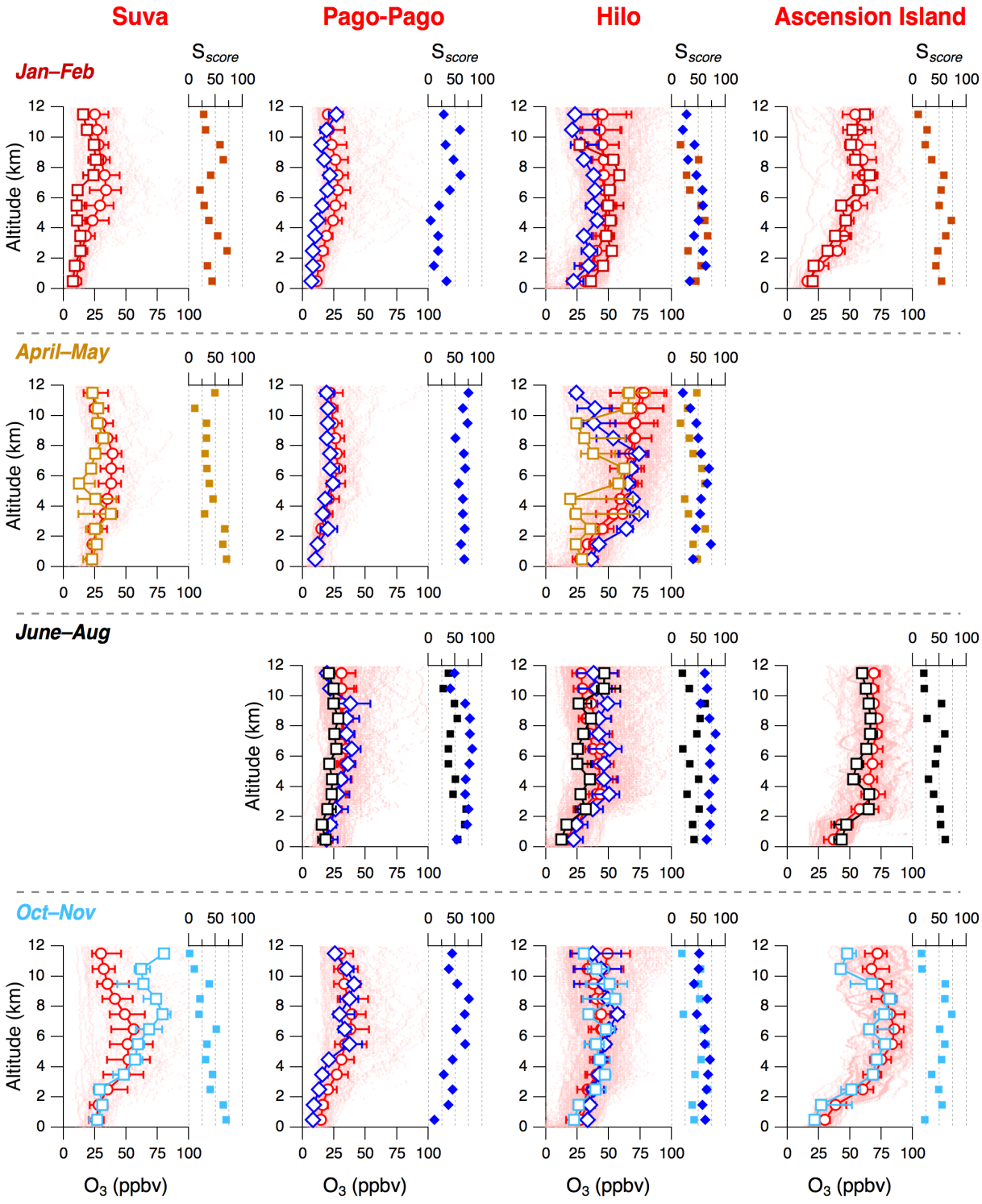

Figure 5 Seasonal comparison of 1 km-vertically-binned ATom (colored squares) and HIPPO (blue diamonds) median O_3 with ozonesonde (red circles) records at four sites in the tropics (Suva in Fiji, Pago-Pago in American Samoa, Hilo in Hawaii, and Ascension Island). Markers indicate the median and the bars are the 25th and 75th percentiles. The S_{score} is a metric of how well ATom

and HIPPO 1 km-binned O_3 probability distribution functions (PDFs) overlap with the corresponding 1 km-binned O_3 PDFs from ozonesondes. The S_{score} shown with squares compares ATom with ozonesondes, and the S_{score} shown with blue diamonds compares HIPPO with ozonesondes. The pink dots show every O_3 data point measured by ozonesondes for the timeframes indicated in Table S2.

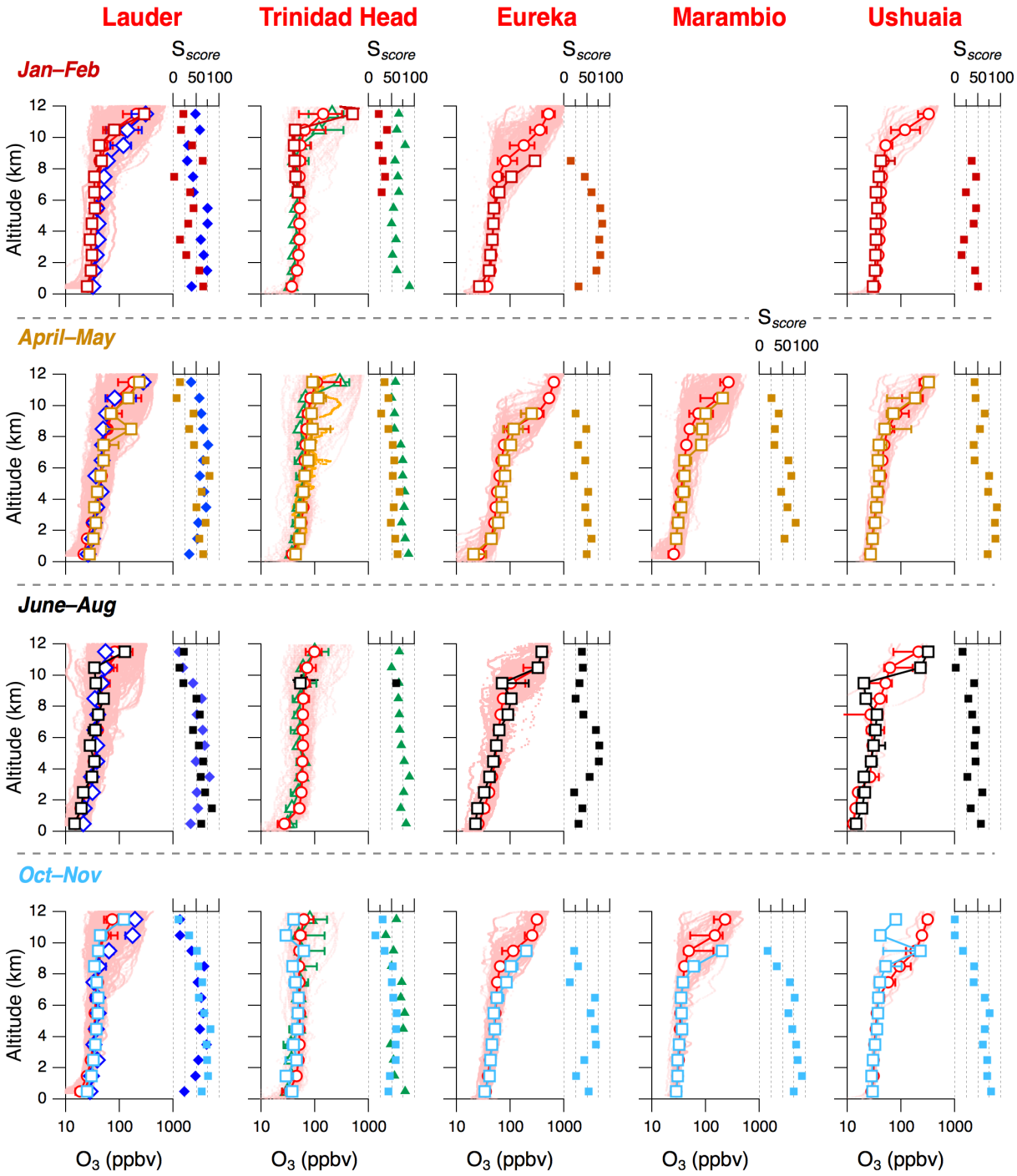

Figure 6 Same as in Figure 5 but for ozonesonde launching sites located in middle- and high-latitudes (Lauder in New Zealand, Trinidad Head in the USA, Eureka in Canada, Ushuaia in Argentina, and Marambio in Antarctica). O_3 data obtained from the IAGOS program (green triangles) during descents into San Francisco Bay-area nearby airports were also added to the Trinidad Head site for comparison.

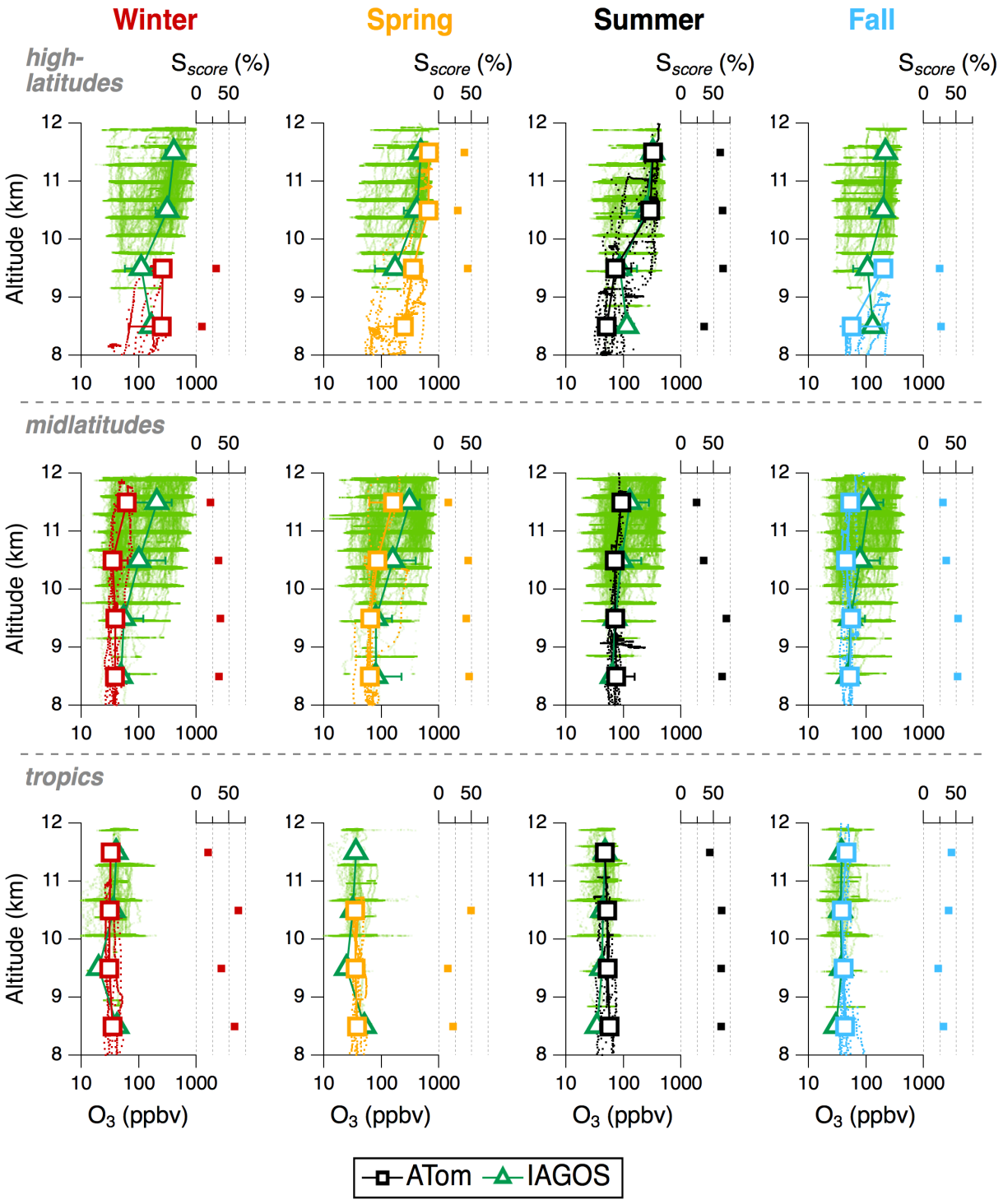

Figure 7 Seasonal comparison of 1 km-binned ATom (colored squares) median O_3 with IAGOS (green triangles) in the northern Atlantic UTLS. Markers indicate the median and the bars are the 25th and 75th percentiles. The three different rows indicate the latitudinal bands. The four columns

indicate the seasons. The green dots show every O_3 data point measured by IAGOS flights for the timeframe indicated in Table S1.

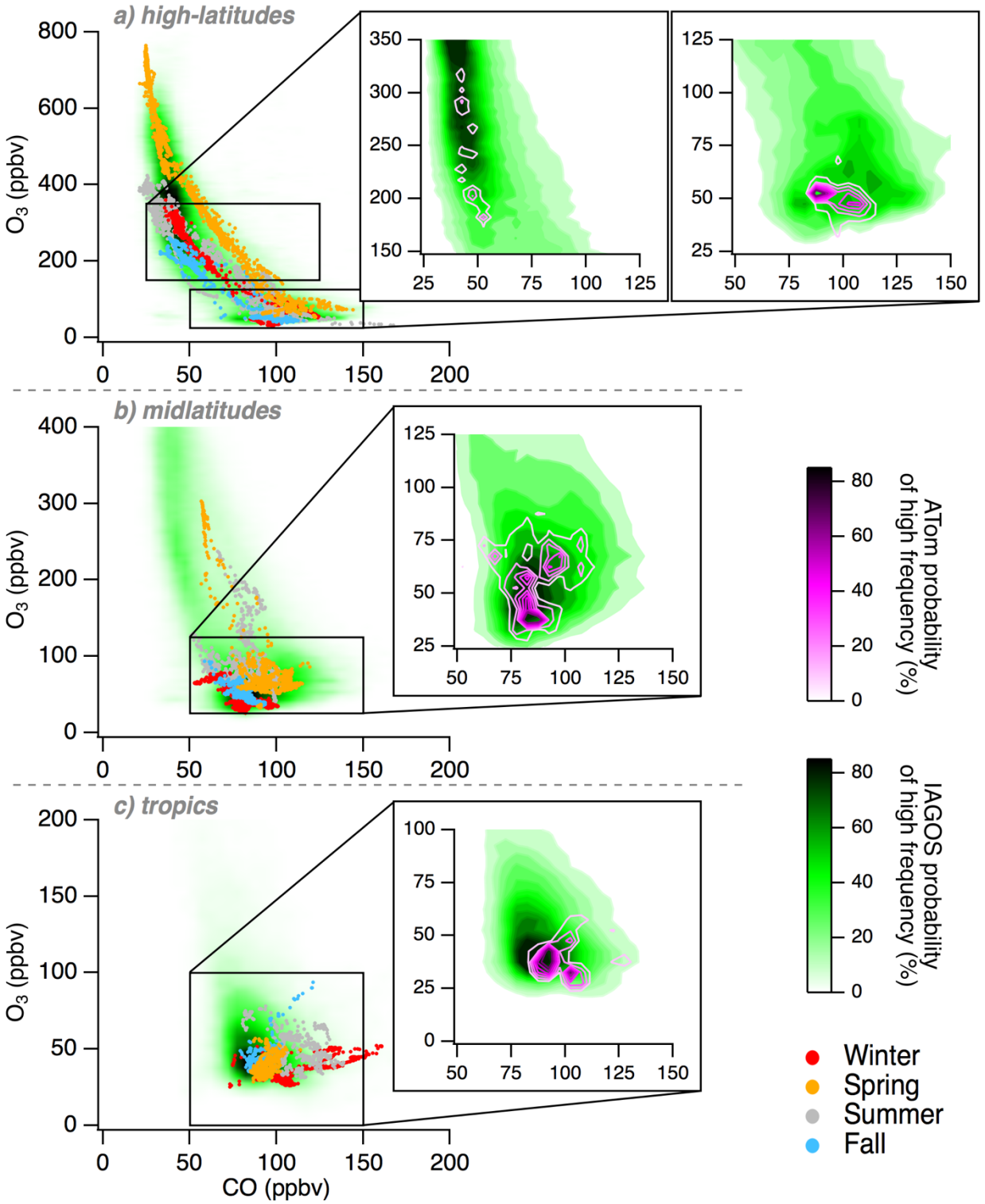

Figure 8 IAGOS and ATom seasonal O_3 vs. CO scatterplots, with insets showing the most frequent O_3 values measured during IAGOS and ATom. ATom seasonal deployments are

colored according to the legend. The frequency gradient of O_3 counts is illustrated by the color scales (green for IAGOS, magenta for ATom). ATom measurements have been combined for the frequency gradients shown in the insets. The probability of high frequency refers to the probability of finding frequently measured O_3 values within the contour boundaries

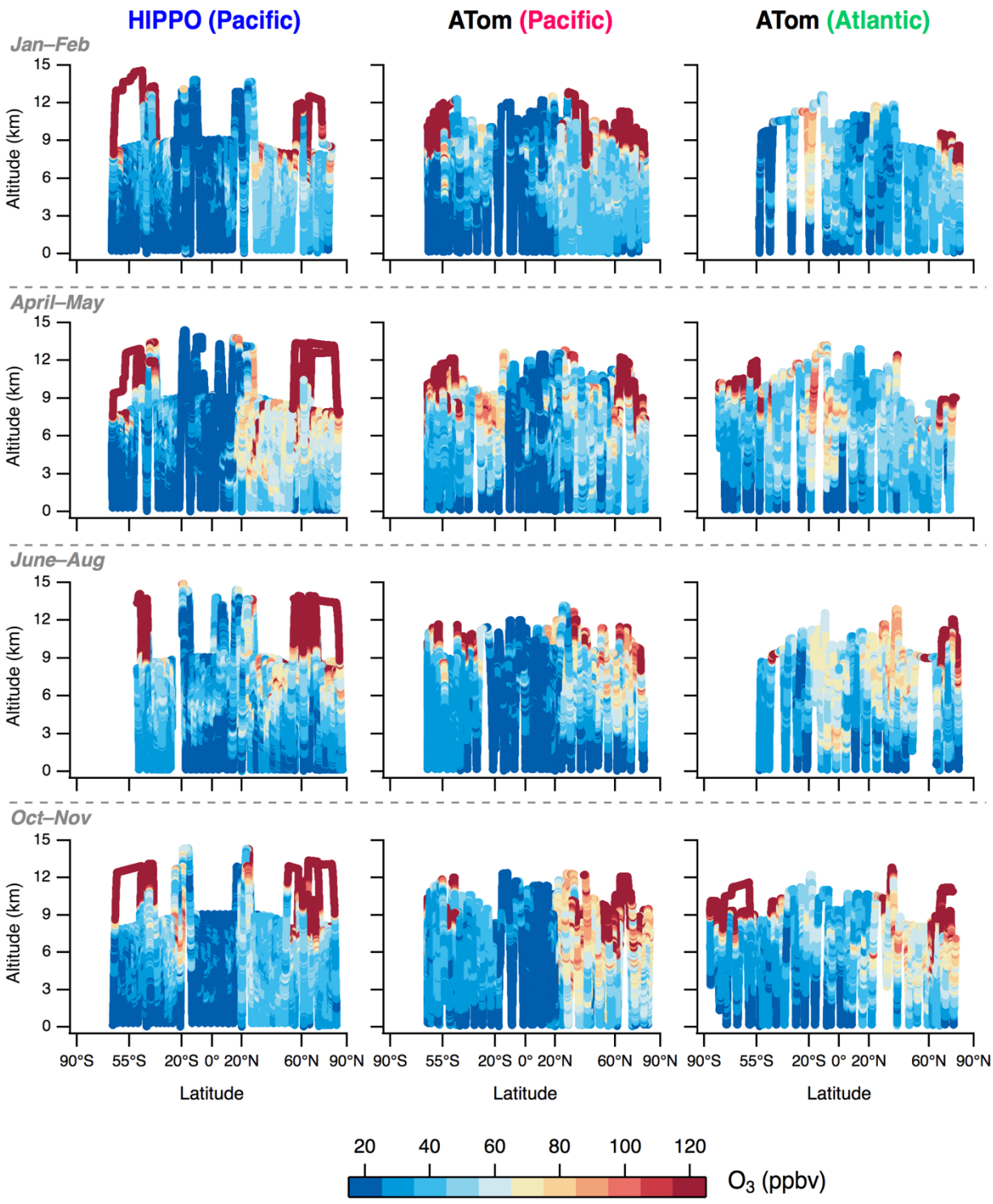

Figure 9 Global-scale distribution of tropospheric O_3 for each ATom and HIPPO seasonal deployment. The rows separate the seasonal deployments, while the columns indicate the mission and the ocean basin. The O_3 color-scale ranges from 20 to 120 ppbv, and all values outside of this

range are shown with the same extremum color (red for values > 120 ppbv, blue for values < 20 ppbv). HIPPO deployments in June and August were combined together.

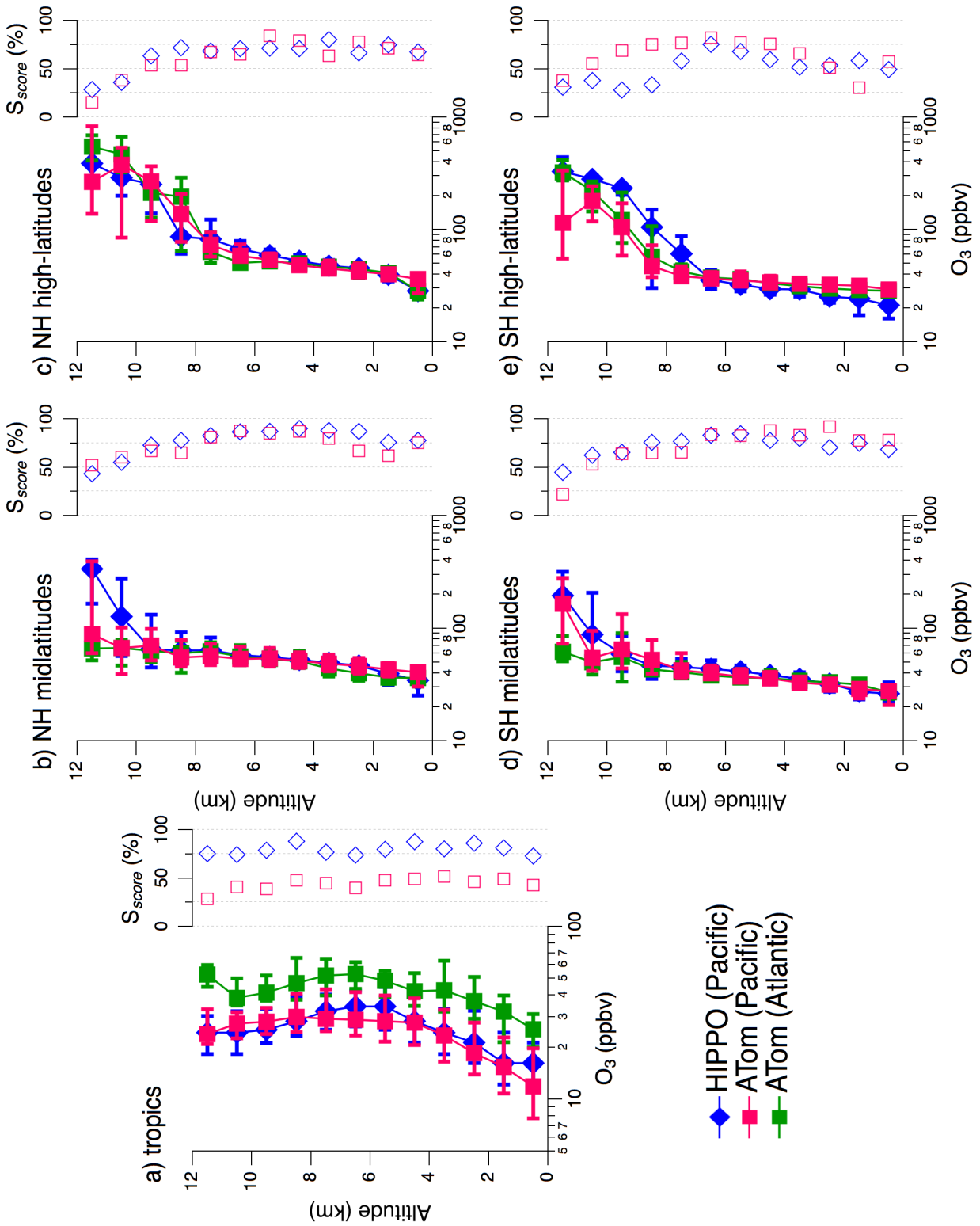

Figure 10 Vertically-resolved O_3 distributions from 0–12 km are plotted for the Atlantic (ATom in green) and for the Pacific (ATom in pink, HIPPO in blue). The five broad latitude regions correspond to the data parsing illustrated by Fig. 1. Markers indicate median O_3, and bars are the

25th and 75th percentiles, per 1 km altitude bin. Note the log scale on the x-axis. S_{score} values resulting from the comparison of HIPPO and ATom Pacific distributions are shown with blue diamonds, and from the comparison of ATom Atlantic and Pacific distributions with pink squares.

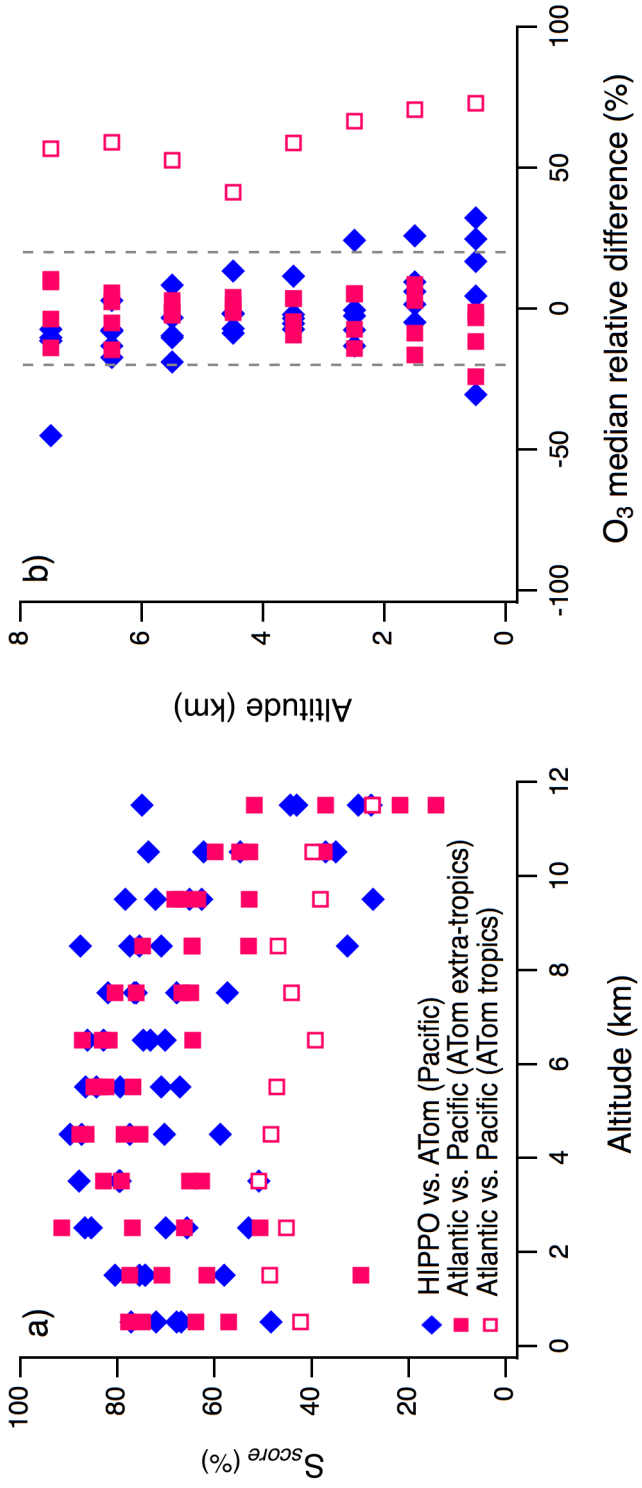

Figure 11 All S_{score} values from Fig. 10 are shown in panel a) and plotted against altitude. The HIPPO and ATom comparison in the Pacific basin is shown with blue diamonds, and a comparison of the Atlantic and Pacific basins during ATom is shown with filled pink squares for the extra-

tropics and open pink squares for the tropics. The relative difference of median O_3 from 0 to 8 km given in Fig. 10 is shown in panel b), with the same color and marker code as in panel a). The dotted grey lines indicate a relative difference of 20 %.

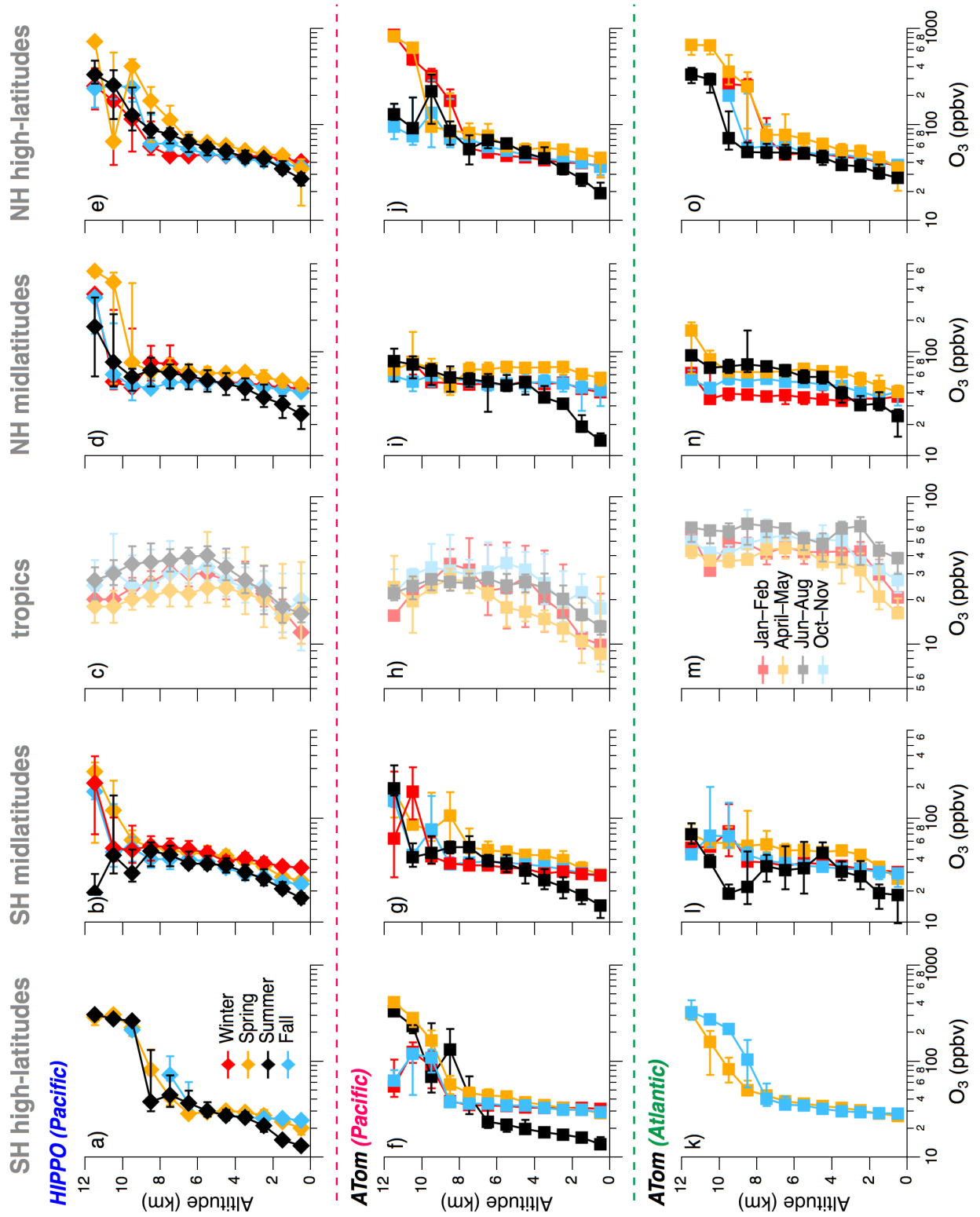

Figure 12 Seasonal variability of regional O_3 distribution in the Pacific (HIPPO in the first and ATom in the second row) and in the Atlantic (ATom in the third row). The colors designate the

local seasons with red as winter, gold as spring, black as summer, and blue as fall (corresponding months are indicated for the tropics, with lighter colors). The markers and associated bars correspond to the median, 25^{th} and 75^{th} percentiles, respectively, of O_3 distribution in every 1 km altitude bin. Note the logarithmic scale on the x-axes in all panels, and the changing scale with latitudinal bin.

Figure 13 O_3 vs. CO plots using combined ATom and HIPPO data. Each panel denotes a different latitudinal band in each basin. Seasonal deployments are colored according to the legend. Note the logarithmic scale on the y-axes in all panels, and the changing scale with latitudinal bin